JGR Atmospheres

RESEARCH ARTICLE
10.1029/2023JD039638

PDO and AMO Modulation of the ENSO–Asian Summer Monsoon Teleconnection During the Last Millennium

Na Wang[1,2], Sylvia Dee[1], Jun Hu[3], Nathan Steiger[4,5], and Kaustubh Thirumalai[6]

[1]Department of Earth, Environmental, and Planetary Sciences, Rice University, Houston, TX, USA, [2]Institute of Atmospheric Physics, Chinese Academy of Sciences, Beijing, China, [3]College of Ocean and Earth Sciences, Xiamen University, Xiamen, China, [4]Institute of Earth Sciences, Hebrew University of Jerusalem, Jerusalem, Israel, [5]Lamont-Doherty Earth Observatory, Columbia University, Palisades, NY, USA, [6]Department of Geosciences, University of Arizona, Tucson, AZ, USA

Abstract Observations show that the teleconnection between the El Niño-Southern Oscillation (ENSO) and the Asian summer monsoon (ASM) is non-stationary. However, the underlying mechanisms are poorly understood due to inadequate availability of reliable, long-term observations. This study uses two state-of-the-art data assimilation-based reconstructions of last millennium climate to examine changes in the ENSO–ASM teleconnection; we investigate how modes of (multi-)decadal climate variability (namely, the Pacific Decadal Oscillation, PDO, and the Atlantic Multidecadal Oscillation, AMO) modulate the ENSO–ASM relationship. Our analyses reveal that the PDO exerts a more pronounced impact on ASM variability than the AMO. By comparing different linear regression models, we find that including the PDO in addition to ENSO cycles can improve prediction of the ASM, especially for the Indian summer monsoon. In particular, dry (wet) anomalies caused by El Niño (La Niña) over India become enhanced during the positive (negative) PDO phases due to a compounding effect. However, composite differences in the ENSO–ASM relationship between positive and negative phases of the PDO and AMO are not statistically significant. A significant influence of the PDO/AMO on the ENSO–ASM relationship occurred only over a limited period within the last millennium. By leveraging the long-term paleoclimate reconstructions, we document and interrogate the non-stationary nature of the PDO and AMO in modulating the ENSO–ASM relationship.

Plain Language Summary Sea surface temperatures in the tropical Pacific oscillate between warmer and cooler conditions every 2–7 years. These oscillations are called "The El Niño-Southern Oscillation (ENSO)" and have been shown to affect weather and climate in remote locations. For example, ENSO has been shown to alter rainfall of the Asian summer monsoon (ASM). However, the connection between ENSO and the ASM is not dependable, making accurate ASM prediction a challenge, especially in a changing climate. Here, we use a new technique that combines geological archives of past climates like ice cores, corals, or lake sediments with climate models to examine alterations in the ENSO–ASM relationship over the past thousand years. In particular, we focus on how other oscillatory ocean temperature patterns, the Pacific Decadal Oscillation (PDO) and the Atlantic Multidecadal Oscillation (AMO), might affect the ENSO–ASM relationship. In the context of the last millennium, we find the differences in the ENSO–ASM relationship between all positive and negative PDO/AMO phases are not statistically significant, as the PDO/AMO modulation on the ENSO–ASM relationship evolves over long time scales. Nevertheless, the PDO itself strongly regulates the Indian summer monsoon, and the consideration of PDO in addition to ENSO enhances monsoon prediction. This information is useful for anticipating decadal-scale changes in the ASM in our changing climate.

Key Points:

- We investigate how the Pacific Decadal Oscillation (PDO) and the Atlantic Multidecadal Oscillation (AMO) modulate the relationship between El Niño-Southern Oscillation (ENSO) and the Asian summer monsoon (ASM) using paleo-data assimilation products
- We find that the PDO impacts ASM variability more than the AMO, and its consideration yields improved Indian summer monsoon predictions
- Notably, the influence of the PDO and AMO on the ENSO–ASM relationship is highly non-stationary across the last millennium

Supporting Information:

Supporting Information may be found in the online version of this article.

Correspondence to:

N. Wang,
nw27@rice.edu

Citation:

Wang, N., Dee, S., Hu, J., Steiger, N., & Thirumalai, K. (2024). PDO and AMO modulation of the ENSO–Asian summer monsoon teleconnection during the Last Millennium. *Journal of Geophysical Research: Atmospheres*, *129*, e2023JD039638. https://doi.org/10.1029/2023JD039638

Received 28 JUL 2023
Accepted 4 DEC 2023

1. Introduction

The Asian monsoon plays a vital role in Earth's climate system, exhibiting a large seasonal shift in prevailing winds (Trenberth et al., 2006). During boreal summer, moisture-laden air crossing the Indo-Pacific Oceans is advected over land, bringing heavy rainfall to coastal areas of East and South Asia (Ding & Chan, 2005; Webster et al., 1998). These monsoon-related rainfall patterns often exhibit substantial year-to-year variations, which produce cascading impacts on local water availability, agriculture, and food security (Gadgil & Rupa Kumar, 2006; Mishra et al., 2012). Predicting Asian summer monsoon (ASM) rainfall under climate change is thus of great significance, but it continues to pose a formidable challenge in climate science (Goswami et al., 2006; Liu et al., 2013; Madolli et al., 2022).

The ASM consists of several sub-systems, including the East Asian summer monsoon (EASM), the Indian summer monsoon (ISM), and the western North Pacific summer monsoon (WNPSM) (Hsu et al., 2014; Wang & LinHo, 2002; Wang et al., 2001). While the WNPSM is known as an oceanic monsoon system, the EASM and ISM are continental monsoon systems and influence freshwater availability directly or indirectly for over one third of the world's population (Ha et al., 2018). Many previous studies indicate an increase in the Asian monsoon rainfall by the end of this century due to continuing anthropogenic warming (Chen et al., 2020; Chevuturi et al., 2018; Hsu et al., 2013; Katzenberger et al., 2021). However, near-term (interannual to decadal-scale) predictions of monsoon rainfall house large uncertainties as a result of internal climate variability, which drives large inter-model spread (Chen et al., 2020).

The El Niño-Southern Oscillation (ENSO) has been extensively investigated as a target for ASM prediction (e.g., George et al., 2016; McGregor et al., 2022; Tang et al., 2018; Webster & Yang, 1992). El Niño events, characterized by elevated sea surface temperatures (SSTs) in the eastern tropical Pacific, are associated with the eastward shift of the Indo-Pacific Walker circulation. This shift leads to increased low-level convergence and upward motion over the equatorial Indian Ocean, and triggers an atypical regional Hadley circulation, characterized by descending motion and reduced rainfall across the Indian subcontinent (Goswami, 1998; Krishnamurthy & Goswami, 2000; Lau & Nath, 2000). Indeed, long-term rainfall records show that droughts in India are frequently observed to coincide with El Niño events (Kumar et al., 2006). The weakened ISM during El Niño events has also been linked to coeval decreased rainfall anomalies in northern China through a circumglobal teleconnection in the middle latitudes (Ding & Wang, 2005; Kripalani & Kulkarni, 2001; Wu, 2002). Conversely, during La Niña years, the ascending branch of the Walker circulation strengthens over the Indo-Pacific region, leading to favorable conditions for increased ISM rainfall (Aneesh & Sijikumar, 2018).

An increasing number of observations and paleoclimate records, however, suggest the ENSO–ASM relationship is non-stationary over time and exhibits decadal-scale variability. For example, ENSO's correlation with ISM rainfall, while usually negative, weakened during the 1970s (Kumar et al., 1999) before recovering in the 21st century (Hu et al., 2022; Yang & Huang, 2021; Yu et al., 2021). With the exception of India, the relationships between ENSO and rainfall in East Asia, Southeast Asia, and the Maritime Continent have all strengthened since the 1950s, contributing to an overall intensification of the ENSO–ASM teleconnection (Wang et al., 2020). Annually resolved paleoclimate reconstructions spanning 1588–2013 C.E. reveal decadal to multidecadal variability of the ENSO–ASM relationship and an enhancement of the relationship since 1850, suggesting the possible influence of anthropogenic forcing (C. Xu et al., 2023; M. Xu et al., 2023). Finally, climate projections suggest that the ENSO–ASM relationship will be further enhanced under greenhouse warming scenarios (Pandey et al., 2020; Roy et al., 2019; Wang et al., 2014).

Many hypotheses have been proposed linking external forcing changes to the coupling between ENSO and ASM systems. For example, Mehta and Lau (1997) proposed that solar irradiance could impact the ENSO–ISM relationship over multidecadal time scales, as a long-lived, above-normal irradiance anomaly would amplify the contrast in thermal conditions between land and sea, leading to an intensification of monsoon winds and above-normal rainfall over India. Recent paleoclimate evidence confirms this, suggesting that during periods of high total solar irradiance, the ENSO-ISM correlation is strengthened and the ENSO-EASM correlation is weakened (Du et al., 2023). In addition, Narasimha and Bhattacharyya (2010) showed ENSO connections with solar activity, and suggested that the influence of solar irradiance on the ISM is indirectly applied via the ENSO teleconnection. Similarly, Jin et al. (2019) suggested that solar activity shapes the decadal variation of the EASM through SST anomalies in the Pacific Ocean. Kumar et al. (1999) attributed the weakening of the ENSO–ISM teleconnection since the 1970s to changes in the Walker circulation and amplified temperature gradients between land and sea, which are linked to global warming. Kim et al. (2016) showed that absorbing aerosols can amplify ENSO's effects on the ISM via a diabatic heating feedback. Finally, Singh et al. (2020) found that large volcanic eruptions can increase the synchronization between ENSO and the Indian monsoon.

While numerous studies have documented the impacts of decadal-scale climate modes, such as the Pacific Decadal Oscillation (PDO) and the Atlantic Multidecadal Oscillation (AMO, also known as the Atlantic Multidecadal Variability) on the ASM (e.g., Chakraborty & Singhai, 2021; Hrudya et al., 2021; Yang et al., 2017), considerably less work has focused on their influences on the interannual relationship between ENSO and the ASM. The PDO is characterized by the interdecadal fluctuation of SSTs and associated circulation changes in the Pacific Ocean. It bears a resemblance to the spatial structures of ENSO, but occurs over longer time scales with a typical period

of 20–30 years (Zhang et al., 1997). Previous studies found that India and southern China are more susceptible to drought conditions when El Niño events occur with positive PDO phases (Chan & Zhou, 2005; Krishnamurthy & Krishnamurthy, 2014; Krishnan & Sugi, 2003). By contrast, wet monsoons tend to be dominant when La Niña events are superimposed on negative PDO phases. However, this primarily illustrates the compound effect of the PDO and ENSO on the ASM. The current research on the PDO's influence on ENSO–monsoon covariability is quite limited, primarily relying on direct comparisons among reconstructed time series (Hau et al., 2023; Shi & Wang, 2019). The AMO is defined as a function of SST fluctuations in the North Atlantic, which have an estimated period of 60–80 years during the observational era (Delworth & Mann, 2000). Both observational and numerical studies indicate that positive AMO phases characterized by anomalously warm North Atlantic SSTs can trigger remote responses in the tropical Pacific Ocean, leading to a decrease in ENSO variability along with the weakening of the ENSO–monsoon teleconnection (Chen et al., 2010; Dong et al., 2006; Fan et al., 2018; C. Xu et al., 2023; M. Xu et al., 2023). It is worth noting that these studies measured monsoon intensity largely based on circulation rather than hydroclimate variability. Still, other work suggests that the non-stationarity in the ENSO–monsoon relationship is simply caused by stochastic perturbations rather than low-frequency deterministic processes (Gershunov et al., 2001; Yun & Timmermann, 2018). Broadly speaking, consensus regarding how these modes of climate variability modulate the ENSO–ASM rainfall relationship is lacking.

The absence of clear constraints on the future of the ENSO–ASM relationship is primarily driven by the inadequate length of and spatial gaps in instrumental observations over the past ∼150 years (which spans only a few PDO and AMO cycles). Whereas paleoclimate records from key regions can help fill in critical temporal gaps, an overall scarcity of coeval paleoclimate data with sufficient spatial coverage in the core ENSO and monsoon regions has heretofore prevented a deeper understanding of the coupling between ENSO and monsoon systems at multi-decadal and longer timescales. To address this, data assimilation of paleoclimate data sets (Paleo-DA) is now widely applied to investigate spatiotemporal patterns of climate variability before the advent of instrumental records (e.g., Bhend et al., 2012; Goosse et al., 2012; Hakim et al., 2016; Steiger et al., 2014; Widmann et al., 2010). By assimilating proxy records with numerical simulations of coupled climate models, Paleo-DA generates globally gridded reconstructions of multiple climate fields simultaneously within a physically consistent framework (Hakim et al., 2016; Steiger et al., 2014, 2018; Tardif et al., 2019a).

This study expands upon the work of several recent papers which have used Paleo-DA products to investigate ENSO characteristics, the response of ENSO dynamics to external forcing, and the ENSO teleconnection in North America during the past 2,000 years (Dee et al., 2020; Dee & Steiger, 2022; Luo et al., 2022, 2023; Steiger et al., 2021; Tejedor et al., 2021). Specifically, we capitalize on the full spatiotemporal information spanning the last millennium at annual resolution afforded by the Paleo-DA products to examine the teleconnection between ENSO and the ASM, with a focus on the modulation of the PDO and AMO on the ASM and the ENSO–ASM teleconnection. We ask the following key questions:

1. What are the individual and compound impacts of ENSO, PDO, and AMO on the ASM over the past millennium?
2. Do the PDO and AMO modulate the variability of the ENSO–ASM relationship?

We use two Paleo-DA reconstructions to evaluate whether inferences surrounding the ENSO–ASM teleconnection drawn from instrumental observations and numerical simulations (Chan & Zhou, 2005; Chen et al., 2010; Dong et al., 2006; Krishnamurthy & Krishnamurthy, 2014; Krishnan & Sugi, 2003) hold over long timescales. Our aim is to provide insights into the dynamics and thus prediction of the ASM in a rapidly changing climate.

2. Materials and Methods

2.1. Data Products

This study uses two Paleo-DA products, the Last Millennium Reanalysis version 2.0 (LMRv2.0, Tardif et al., 2019a) and the Paleo Hydrodynamics Data Assimilation Product (PHYDA, Steiger et al., 2018). Both the LMRv2.0 and PHYDA combine paleoclimate proxies and coupled climate models to yield an optimal estimate of past climate over the Common Era (0–2000 C.E.). LMRv2.0 utilized the Community Climate System Model version 4 Last Millennium simulation (CCSM4-LM, Landrum et al., 2013) as a model prior and assimilated temperature-sensitive proxies from the PAGES2k database (Emile-Geay et al., 2017), along with additional data provided by Anderson et al. (2019). PHYDA was based on a hydroclimate-sensitive proxy network consisting of

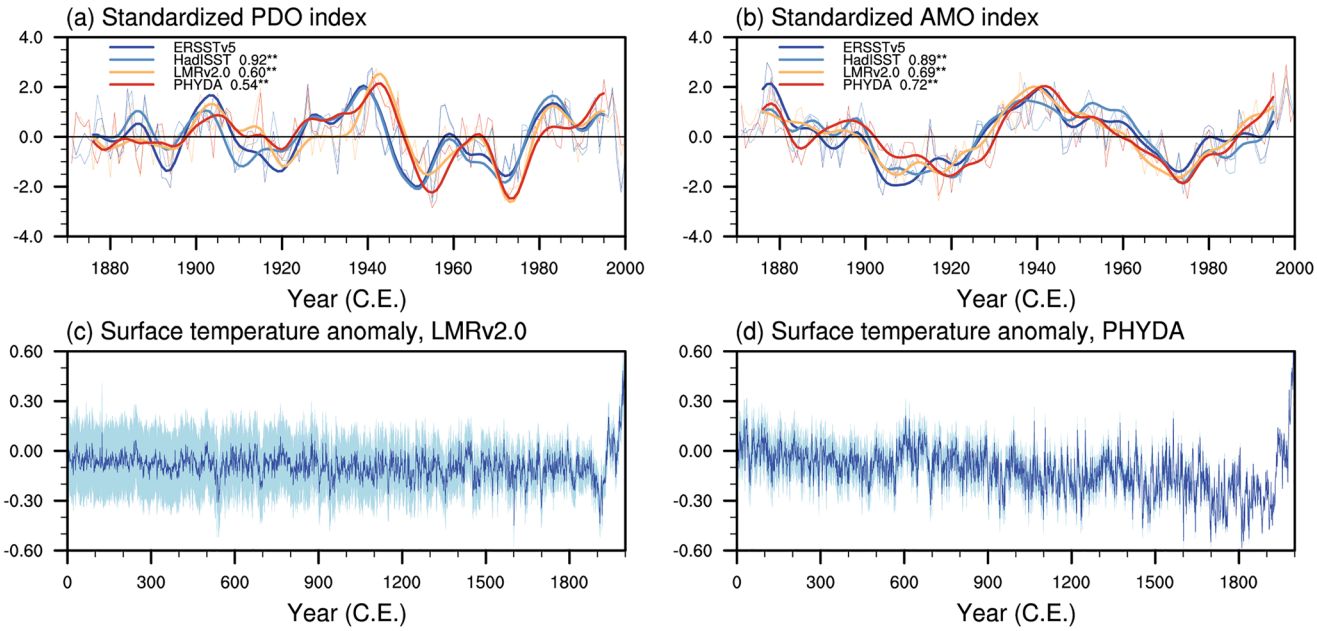

Figure 1. Validation of the PDO and AMO indices and uncertainties of temperature reconstructions. (a) Standardized PDO and (b) AMO indices for 1871–2000 C.E. calculated from ERSSTv5, HadISST, LMRv2.0, and PHYDA. Correlations between ERSSTv5 and other data sets are shown in the upper left corner, with ** signifying statistical significance at the 99% confidence level using the Student's *t*-test. Solid lines denote the 20-year lowpass filtered time series. (c, d) Global mean surface temperature anomaly for 0–2000 C.E., relative to the average of 1951–1980 C.E. from (c) LMRv2.0 and (d) PHYDA ensemble mean. The corresponding ±1σ ranges for 100 ensemble members and 20 Monte-Carlo realizations of LMRv2.0 and 100 ensemble members of PHYDA are shown in light blue, indicating the range of uncertainties associated with the temperature reconstructions.

2978 proxy time series (Steiger et al., 2018), and employed the Community Earth System Model Last Millennium Ensemble (CESM-LME, Kay et al., 2015) as the climate model prior.

Although LMRv2.0 and PHYDA provide reconstructions spanning the past two thousand years, the amount of paleoclimate proxies assimilated decreases over time, resulting in smaller variances and larger uncertainties in the reconstructed climate variables, especially in the first half of the Common Era (Steiger et al., 2018, also shown in Figures 1c and 1d). We thus restrict our analysis to the period between 851 C.E. and 1950 C.E., which we refer to as the last millennium in this study. The starting point of 851 C.E. is selected to facilitate convenient comparison with the CESM-LME simulations; 1950 C.E. is selected as the endpoint to reduce the influence of anthropogenic forcing caused by carbon emissions from fossil fuels.

We use the ensemble mean of climate fields in the annually resolved, globally gridded reconstructions from the Paleo-DA products. The LMRv2.0 reconstructs annual mean variables from January to December, whereas the annual mean for PHYDA is defined as April to the following March of the calendar year. The LMRv2.0 global gridded data contains SST, 2 m surface temperature, sea level pressure, 500-hPa geopotential height, precipitation rate, precipitable water, and the Palmer drought severity index (PDSI). The PDSI is a standardized drought index, with positive (negative) values representing wet (dry) conditions (Palmer, 1965). PHYDA provides three global variables: 2 m surface temperature, the PDSI, and the standardized precipitation evapotranspiration index. Since PDSI is the only hydroclimate variable provided by both LMRv2.0 and PHYDA, we use it as a metric for monsoon rainfall for ease of comparison. We use SST from LMRv2.0 and 2 m surface temperature from PHYDA to calculate the ENSO, PDO, and AMO indices. Note SST and 2 m surface temperature are identical over the open ocean, and the correlation coefficients between the ENSO, PDO, and AMO indices derived from the SST and 2 m surface temperature data approach 1.0, confirmed through testing with LMRv2.0 (not shown).

To validate the performance of LMRv2.0 and PHYDA in reproducing the ENSO–ASM teleconnection and decadal-scale climate variability, we employ both instrumental observations and modern reanalysis data sets. Specifically, we use SST data from the Hadley Centre Global Sea Ice and Sea Surface Temperature (HadISST, Rayner et al., 2003) and the Extended Reconstructed Sea Surface Temperature version 5 (ERSSTv5, Huang et al., 2017a), and PDSI from Dai (2011) computed from observed monthly surface air temperature and

precipitation. To maintain consistency when comparing with reconstructions, we follow the methodology employed in PHYDA by calculating the annual mean of observations as the average from April to the following March.

Climate model simulations from the CESM-LME full forcing experiments are analyzed as a supplement for comparison with the Paleo-DA products (Kay et al., 2015; Otto-Bliesner et al., 2016). The CESM-LME full forcing simulations were conducted with version 1.1 of CESM for the period 850–2005 C.E., forced with the time-varying solar intensity, volcanic eruptions, land use conditions, greenhouse gasses, aerosols, and orbital parameters (Otto-Bliesner et al., 2016). We primarily use the precipitation and SST outputs from all available 13 members of the CESM-LME full forcing simulations to replicate the analyses conducted using the PDSI and SST/2 m surface temperature reconstructions from Paleo-DA products.

2.2. Study Regions and Index Definitions

This study aims to examine the ENSO teleconnection with the continental components of the ASM. Given the significant spatial differences in precipitation variability within the monsoon region (Wang et al., 2018), we focus on the reconstructed PDSI variability over the core regions of the ISM and EASM, where the maximum monsoon rainfall or rainfall belt is located. The ISM core region is defined as 18°N–25°N and 65°E−88°E, following Rani et al. (2021). For the EASM, the core region is defined as 27°N–35°N and 105°E−125°E, covering the Meiyu-Baiu rainfall belt (Wang et al., 2008). These core regions are denoted with black rectangles in Figure 2. Note that although marine areas are technically contained in the rectangular regions defined for the ISM and EASM, we only utilize terrestrial PDSI data in our calculations.

We characterize ENSO variability using the NINO3.4 index, which is calculated by subtracting the long-term average from the annually resolved SST reconstructions, and averaging SST anomalies over the region of 5°N–5°S, 170°W–120°W (Trenberth, 1997).

The PDO index is defined as the leading principal component of the area-weighted North Pacific SST anomalies over the region of 20°N–66°N, 100°E−100°W (Mantua et al., 1997; Zhang et al., 1997). Considering the notable warming trend during the validation period (1871–2000 C.E.) and the overall cooling trend over the past millennium (Hakim et al., 2016), a detrending step is initially applied to the temperature data prior to PDO index computation. This involves subtracting the smoothed temperature from the original data at each grid point. Specifically, we utilize the Locally Weighted Scatterplot Smoothing (LOWESS) method (Cleveland, 1979) with a window length of 100 years.

The AMO index is defined as the area-weighted North Atlantic SST anomalies over the region of 0–60°N, 0–80°W (Trenberth & Shea, 2006). Similar to the PDO index, we use the detrended SST anomalies to calculate the AMO index.

2.3. Statistical Methods

In this study, we employ El Niño and La Niña events and the positive and negative phases of the PDO and AMO and use composite analysis to distinguish differences between the opposing events/phases. Wavelet analysis of the NINO3.4, PDO, and AMO time series spanning the last millennium revealed multi-scale temporal variability (Figure S1 in Supporting Information S1). To separate interannual from decadal and longer time scale variability, we applied a 2–7-year bandpass filter to the NINO3.4 index and a 20-year lowpass filter to the PDO and AMO indices. El Niño (La Niña) events are identified when the bandpass-filtered NINO3.4 index exceeds (falls below) 0.5 standard deviations from the mean. Positive (negative) phases of the PDO and AMO are defined as years when the lowpass-filtered PDO and AMO indices exceeds (falls below) 0.5 standard deviations from their respective means. Given the potential overlapping and counterbalancing influences of the PDO and AMO phases, we only include non-overlapping years in our composite analysis (see Figure S2 in Supporting Information S1 for the resulting PDO and AMO phases used in the composite analysis). When a year satisfies both an El Niño event definition and a positive PDO phase definition, we define it as an El Niño occurring during the positive PDO phase. Accordingly, we can identify El Niño and La Niña events that occur during positive and negative PDO and AMO phases.

We use the moving correlation coefficients between the NINO3.4 index and the regionally-averaged PDSI over the ISM and EASM core regions to quantify the temporal evolution of the ENSO–ISM and ENSO–EASM

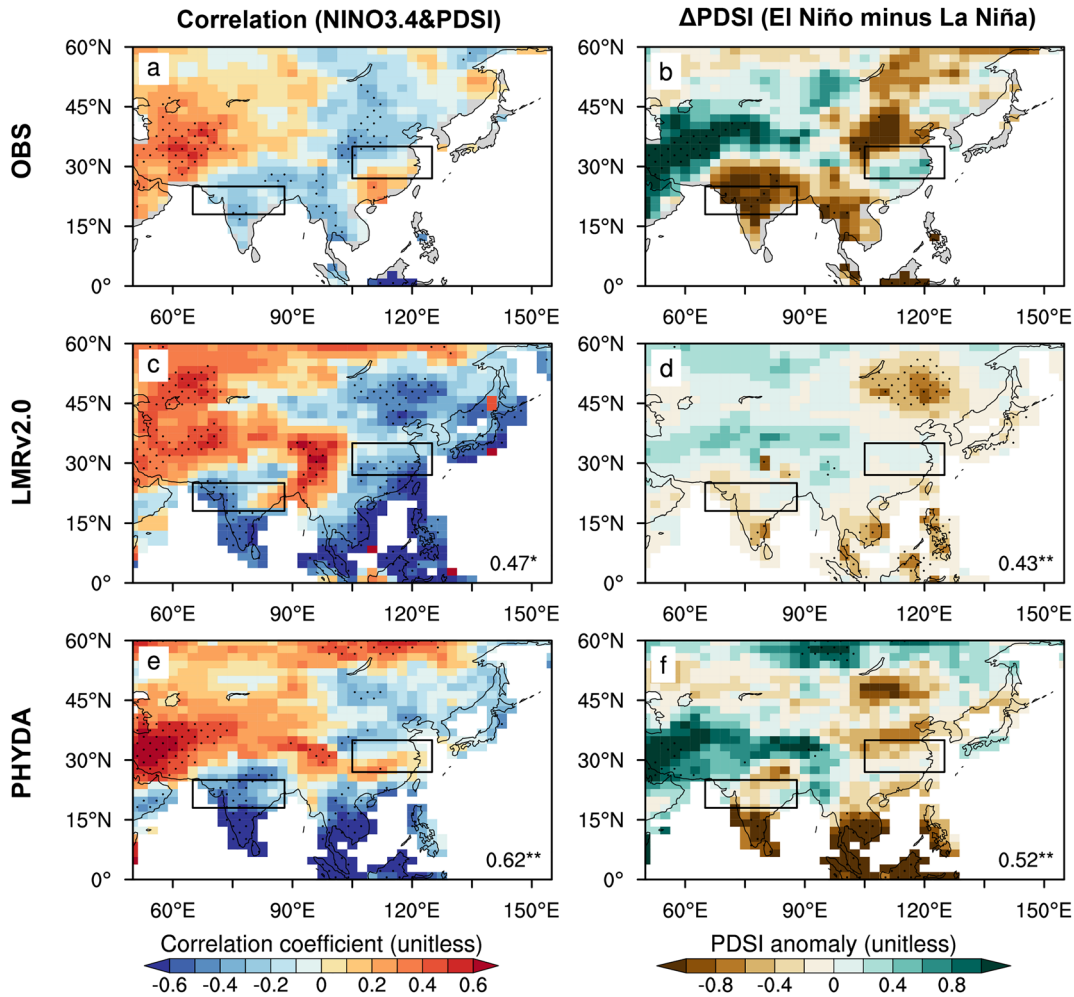

Figure 2. Validation of the ENSO–ASM relationship during the instrumental period. Left column (a, c, e): Correlation coefficients between the NINO3.4 index and PDSI for 1951–2000 C.E., calculated from (a) ERSSTv5 observations and Dai PDSI index, (c) LMRv2.0, and (e) PHYDA. Right column (b, d, f): Differences in PDSI composites between El Niño and La Niña events for 1951–2000 C.E, calculated from (b) ERSSTv5 observations and Dai PDSI index, (d) LMRv2.0, and (f) PHYDA. Dotted areas denote significant results at the 95% confidence level. Black boxes represent the core regions of the EASM and ISM. The number displayed at the bottom right of panels (c–f) represents the spatial correlation between the Paleo-DA products and the corresponding observations over 0°–60°N, 50°E−155°E; ** (*) denotes statistical significance at the 99% (95%) confidence level using the Student's *t*-test.

relationship. To capture detailed variations in these relationships, we use a relatively short sliding window of 21 years, following previous studies (e.g., Chen et al., 2010; Fan et al., 2017). We also confirmed that results are similar when we change the sliding window sizes to 31 years or 51 years (Figure S3 in Supporting Information S1).

Linear regression analyses are conducted using various combinations of the NINO3.4, PDO, and AMO indices to differentiate their influences on the ASM variability. In the regression analyses, we utilized the indices in their raw, unfiltered form to ensure indices incorporate both low-frequency and high-frequency variability.

Finally, we use a two-tailed Student's *t*-test for evaluating the significance of both the composite difference analyses and correlation analyses. To address the potential impact of autocorrelation on the sample sizes, we employ Equations 1 and 2 to calculate effective sample sizes for the difference test and correlation test, respectively (Afyouni et al., 2019; Zwiers & Storch, 1995).

$$N_e = N\frac{1-r_1}{1+r_1} \quad (1)$$

where N represents the original sample size, and r_1 denotes the lag-1 autocorrelation.

$$N_e = N\left(1 + 2\sum_{i=1}^{M}\frac{N-k}{N}r_{x,k}r_{y,k}\right)^{-1} \quad (2)$$

where N represents the original sample size, M is the cut-off lag determined by $N/5$, and $r_{x,k}$ and $r_{y,k}$ stand for the lag-k autocorrelations of the time series.

3. Results

We first assess the performance of the two Paleo-DA products in reproducing the PDO and AMO and the relationship between ENSO and the ASM during the instrumental period (Section 3.1). We then conduct composite analysis to investigate the influence of ENSO/PDO/AMO phase changes on the ASM in the context of the last millennium (Section 3.2), as well as the compound impacts of the PDO/AMO and ENSO on the ASM (Section 3.3). Additionally, we examine the influence of the PDO/AMO on the ENSO–ASM relationship, or teleconnection strength (Section 3.4). Note Sections 3.3 and 3.4 represent two entirely distinct analyses: Section 3.3 focuses on the ASM rainfall variability, while Section 3.4 delves into the covariability between ENSO and the ASM. Finally, we explore potential mechanisms for PDO and AMO impacts on the ASM (Section 3.5).

3.1. Validation of Paleoclimate Data Assimilation Products

To validate the PDO and AMO index time series reconstructed in LMRv2.0 and PHYDA, Figure 1 shows a comparison of both products to instrumental observations. Both reconstructions underestimate PDO variability prior to the 20th century, and the phasing of the reconstructed PDO lags that of the observed PDO between 1940 and 1970 C.E. However, the correlation between the reconstructed and observed PDO indices exceed 0.50 (0.60 for LMRv2.0 and 0.54 for PHYDA) for the period 1871–2000 C.E., and all are significant at the 99.9% confidence level, even when accounting for reduced degrees of freedom due to autocorrelation. Correlations between the reconstructed and observed AMO indices are even higher, reaching 0.69 in LMRv2.0 and 0.72 in PHYDA. Both Paleo-DA products capture main characteristics of the instrumental AMO index across the 20th century. We thus assert that LMRv2.0 and PHYDA reasonably reproduce the decadal-scale variability of the AMO and PDO over the past century.

Previous studies have confirmed the reliability of ENSO and the Asian hydroclimate reconstructions in the LMRv2.0 and PHYDA data sets (see Supporting Information S1 of Hu et al., 2023; Luo et al., 2022). The reconstructed SST pattern related to ENSO and the time series of the NINO3.4 index closely resemble observations of the 20th century (see Figures S2 and S3 in Luo et al., 2022). Reconstructed PDSI over the Asian monsoon regions is positively correlated with reanalysis PDSI from Dai (2011), though we note that the PDSI of both Paleo-DA products is more reliable in central-northern China than in southern China and northeastern India (Hu et al., 2023).

We further compare the ENSO–ASM teleconnection in LMRv2.0 and PHYDA to the teleconnection as characterized by instrumental observations between 1951 and 2000 C.E. (Figure 2). The observations demonstrate an overall anti-correlation of the PDSI in the ASM regions with the NINO3.4 index, and significant negative correlations are found in the ISM region, Southeast Asia, and northern China (Figure 2a). Positive correlations between the NINO3.4 index and PDSI emerge across parts of southern China, but no significant correlation exists in most of the EASM region. Differences in the PDSI composites (Figure 2b) are consistent with the correlation analysis, indicating that during El Niño years, the ISM region, Southeast Asia, and northern China experience drier conditions compared to La Niña years, while southern China becomes relatively wetter. Notably, the PDSI changes in southern China are statistically insignificant. Both LMRv2.0 and PHYDA capture the overall inverse relationship between the NINO3.4 index and PDSI in the ASM regions (Figures 2c–2f), although the performance in East Asia is weaker than in South Asia. The discrepancy between observations and Paleo-DA reconstructions in East Asia results from the scarcity of proxy data in this region and the inherently weak ENSO–EASM relationship evident in observations. Nevertheless, the spatial correlations between reconstructions and observations are higher than 0.4 across the region bracketed by 0°–60°N, 50°E−155°E, and are all significant at least at the 95% confidence level. PHYDA better reproduces the spatial pattern of the ENSO–ASM teleconnection compared to LMRv2.0.

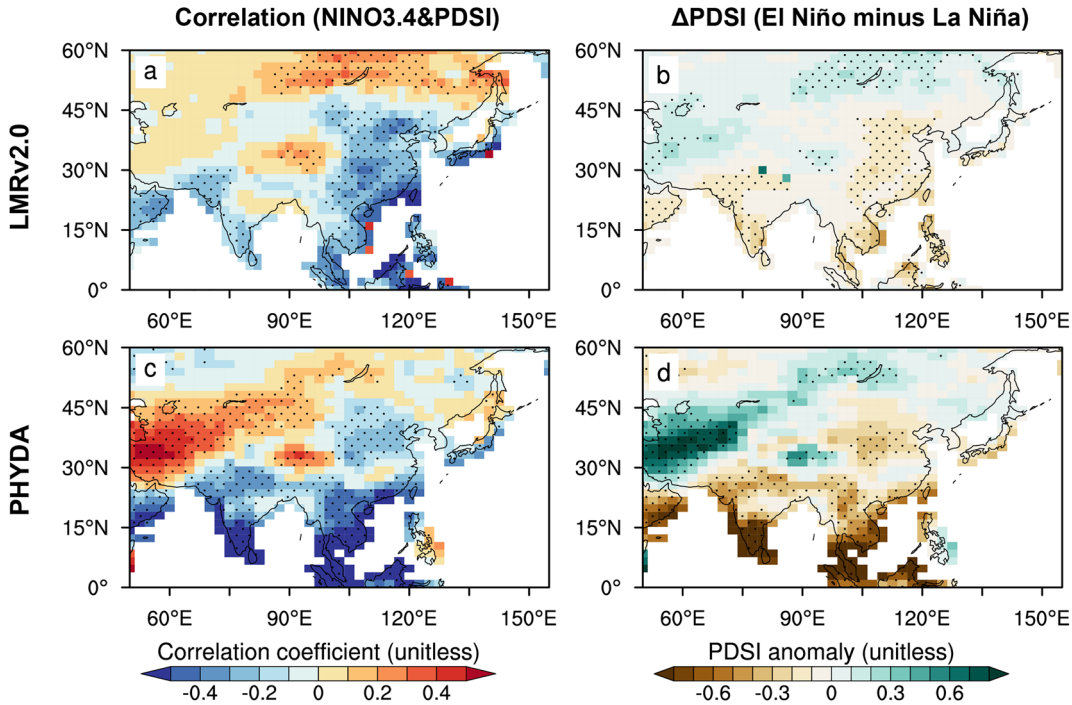

Figure 3. Reconstruction of the ENSO–ASM relationship over the last millennium. Left column: Correlation coefficients between the NINO3.4 index and PDSI for 851–1950 C.E., calculated from (a) LMRv2.0, and (c) PHYDA. Right column: Differences in PDSI composites between El Niño and La Niña events for 851–1950 C.E., calculated from (b) LMRv2.0, and (d) PHYDA. Stippled areas denote significant results at the 95% confidence level using the Student's *t*-test.

3.2. Individual Impacts of ENSO, PDO, and AMO on the Asian Summer Monsoon

The ENSO–ASM relationship during the last millennium is consistent with that of the instrumental period (Figure 3). The results from LMRv2.0 indicate an inverse relationship between the NINO3.4 index and PDSI across most of the ASM regions, except for the coastal area of the northern Bay of Bengal. Correlation coefficients are higher in the EASM region compared to the ISM region in LMRv2.0. PHYDA also shows a negative correlation between the NINO3.4 index and the PDSI in most of the ASM regions except for the Yangtze River Valley, with stronger correlations in the ISM region compared to the EASM region. In accordance with the correlation analysis, PDSI decreases in most of the ASM regions when La Niña shifts to El Niño, except for the coastal area of the northern Bay of Bengal in LMRv2.0 and the Yangtze River Valley in PHYDA. CESM-LME ensemble members consistently show that the precipitation response to ENSO in the core region of the EASM (covering the Yangtze River Valley) and northeastern India is opposite to that of other ASM regions (Figure S4 in Supporting Information S1). Across transitions from La Niña to El Niño events, the simulated precipitation in the EASM core region and northeastern India increases; by contrast, precipitation decreases in northern China, Southeast Asia, and southern India. In general, the CESM-LME and both Paleo-DA products show that the shift from La Niña to El Niño results in drier conditions in northern China, Southeast Asia, and India.

Both Paleo-DA products reveal that the spatial pattern of the ASM as influenced by the PDO resembles that of ENSO over the past millennium (Figures 4a and 4c). During positive PDO phases, the ASM regions generally experience drier conditions, while the negative PDO leads to wetter conditions. Significant signals are observed in most monsoon regions except for eastern China. By contrast, the PDSI within the ASM regions exhibits no discernible response to changing phases of the AMO with the exceptions of eastern India and southeast Asia in PHYDA, where PDSI decreases during positive phases of the AMO (Figures 4b and 4d).

The majority of CESM-LME simulations show no significant precipitation response to the PDO in eastern China and northeastern India (Figure S5 in Supporting Information S1). Meanwhile, a significant decrease in precipitation occurs in other ASM regions when PDO transitions from its negative phase to its positive phase. The majority of CESM-LME members show that the impact of the AMO on the ASM is minimal (Figure S6 in Supporting Information S1).

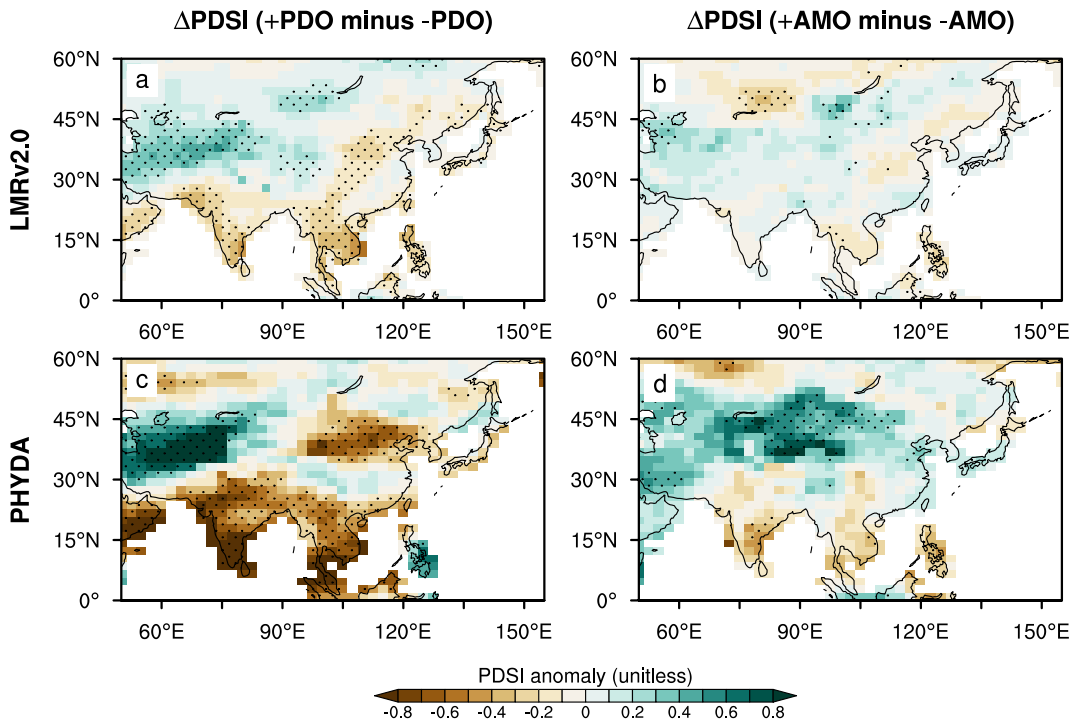

Figure 4. Individual impacts of PDO/AMO on the ASM. Differences in PDSI composites between positive and negative phases of the (a, c) PDO and (b, d) AMO for 851–1950 C.E., calculated from (a, b) LMRv2.0, and (c, d) PHYDA. Stippled areas denote significant differences at the 95% confidence level using the Student's *t*-test.

3.3. Compound Impacts of the PDO/AMO and ENSO on the Asian Summer Monsoon

The previous section evaluates the influence of ENSO, PDO, and AMO on the ASM separately. El Niño and La Niña events, alternately occurring as interannual variability, are superimposed on the decadal-scale variations of the PDO and AMO. In this section, we focus on El Niño and La Niña events that occur during certain phases of the PDO/AMO, and examine whether the ASM anomalies related to the compound impacts of PDO/AMO and ENSO *are distinct* from the ASM anomalies when considering ENSO alone. Specifically, we compare differences in the PDSI composites between El Niño (La Niña) events that occur during a certain phase of the PDO/AMO with all El Niño (La Niña) events over the entirety of the last millennium. For the compound effect of the PDO and ENSO, there are four combinations in total: El Niño + positive PDO phase, La Niña + positive PDO phase, El Niño + negative PDO phase, and La Niña + negative PDO phase; the same is true for the AMO.

When El Niño or La Niña events occur with a positive PDO phase, the PDSI over ASM regions overall *decreases* relative to the average PDSI response to all El Niño or La Niña events (Figure 5). Notably, significant drying signals are only present in southern India and Southeast Asia during La Niña + positive PDO events for the LMRv2.0. PHYDA reveals significant dryings in northern China and India during El Niño + positive PDO events; during La Niña + positive PDO events, significant dryings are limited to India alone. By contrast, when El Niño or La Niña events occur with a negative PDO phase, the PDSI over the ASM regions overall *increases* relative to the average PDSI response to all El Niño or La Niña events. Both LMRv2.0 and PHYDA show significantly wetter conditions in northern China, India, and Southeast Asia during El Niño + negative PDO events. By contrast, shifts towards wetter conditions are mostly insignificant during La Niña + negative PDO events. Given that the El Niño (La Niña) events are associated with decreased (increased) PDSI in most of the ASM regions (Figure 3), PHYDA and LMRv2.0 reconstructions consistently suggest that during the positive phases of the PDO, the El Niño (La Niña) effect on the ASM is enhanced (weakened). Conversely, during the negative phases of the PDO, the La Niña (El Niño) effect is enhanced (weakened). Both LMRv2.0 and PHYDA show that the ASM anomalies due to the compounding effects of AMO and ENSO do not differ significantly from the ASM anomalies when considering ENSO alone (Figure 6). Most CESM-LME members show that when El Niño or La Niña events are superimposed on the positive or negative phases of the PDO and AMO, the

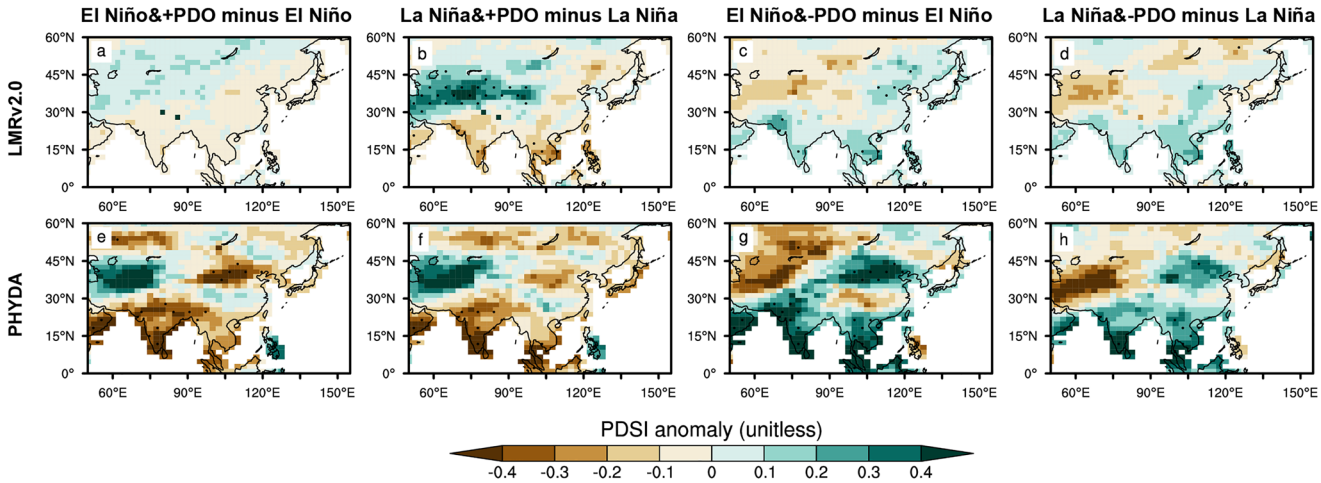

Figure 5. Compound impacts of PDO and ENSO on the ASM relative to the average impacts of ENSO. Differences in PDSI composites between (a, e) El Niño events under positive PDO phases and all El Niño events, (b, f) La Niña events under positive PDO phases and all La Niña events, (c, g) El Niño events under negative PDO phases and all El Niño events, (d, h) La Niña events under negative PDO phases and all La Niña events for 851–1950 C.E., calculated from (a–d) LMRv2.0, and (e–h) PHYDA. Dotted areas denote significant differences at the 95% confidence level using the Student's *t*-test.

resulting precipitation anomalies in the ASM regions do not significantly differ from the average precipitation anomalies of all El Niño and La Niña events (Figures S7–S14 in Supporting Information S1).

Based on the Paleo-DA reconstructions, we find that the PDO exerts a stronger influence on the ASM compared to the AMO. Furthermore, the PDO has a more pronounced impact on the ISM compared to the EASM. To further validate this result, we constructed linear regression models using the regionally-averaged PDSI over the EASM and ISM regions as the dependent variables and NINO3.4, PDO, and AMO indices as predictor variables (Figure 7). A comparison of the goodness of fit of different regression models, measured by the adjusted R-squared values, indicates that adding the AMO as a predictive factor beyond the NINO3.4 index does not measurably improve the prediction skill for the EASM and ISM (Figures 7a and 7b). However, incorporating the PDO significantly improves the prediction skill for the ISM (Figure 7b). It should be noted that the adjusted R-squared values of these linear regression models are too small to be used for practical monsoon predictions. Here, our main objective is to distinguish the relative importance of the PDO and AMO on the East Asian and Indian monsoons by comparing the adjusted R-squared values of different regression models. From the perspective of partial regression correlations, the PDO contributes even more significantly to the variability of the ISM than ENSO variability in the multiple linear regression (Figure 7c). This aligns with our current understanding of the

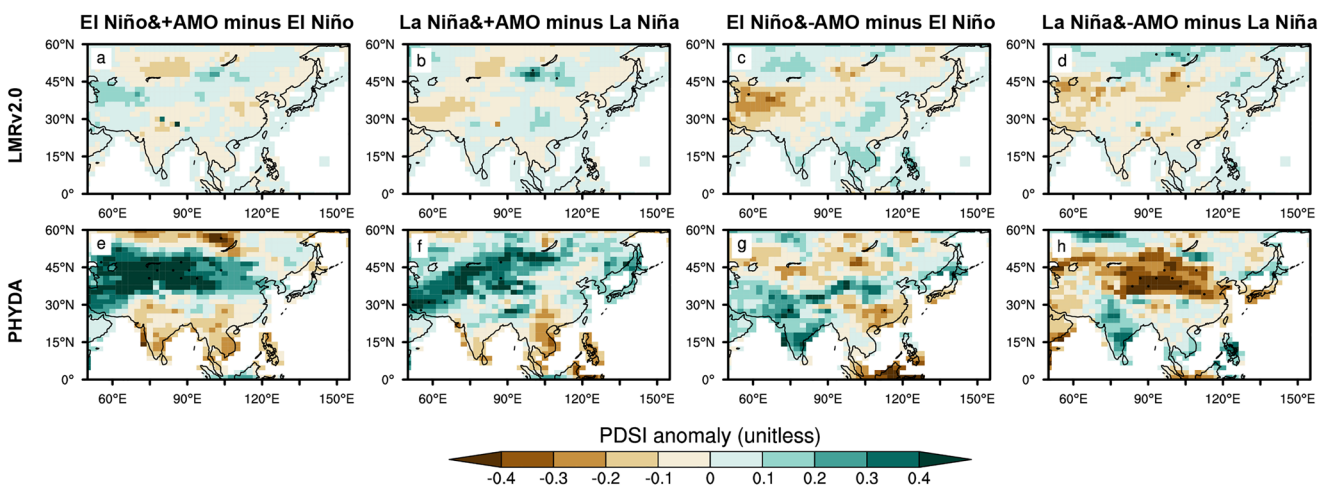

Figure 6. Same as in Figure 5, but for the compound impacts of AMO and ENSO on the ASM relative to the average impacts of ENSO.

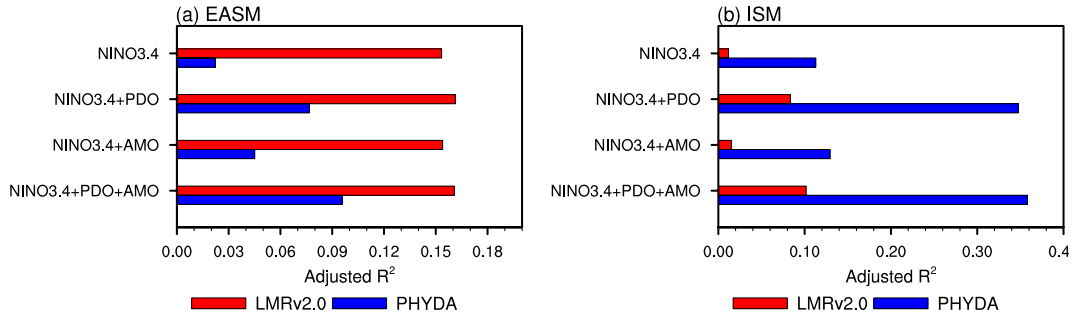

(c) Partial regression coefficients

	EASM		ISM	
	LMRv2.0	PHYDA	LMRv2.0	PHYDA
NINO3.4	-0.09**	-0.17**	-0.001	0.03
PDO	-0.03**	0.12**	-0.09**	-0.37**
AMO	-0.004	0.07**	0.04**	-0.07**

Figure 7. Regression of the regional mean PDSI on NINO3.4, PDO, and AMO indices. (a, b) Adjusted R-squared values for the linear regression models of regional mean PDSI over the (a) EASM and (b) ISM regions using different predictive factors. A larger adjusted R-squared value indicates a better fit of the regression model to the data. (c) Partial regression coefficients of the multivariable linear regression model of EASM and ISM using the standardized NINO3.4, PDO, and AMO indices as predictive factors, which measure the individual contribution of each predictive factor to the regression model. ** denotes statistical significance at the 99% confidence level using the Student's *t*-test.

PDO as a product of multiple processes, encompassing both remote tropical forcing and local ocean–atmosphere interactions in the midlatitudes (Newman et al., 2016).

3.4. Influence of the PDO/AMO on the ENSO–Monsoon Relationship

We also examine the impact of the PDO/AMO on the strength of the teleconnection between ENSO and the ASM. For both subsystems of the ASM, the EASM and ISM, we calculate the 21-year moving correlations between the regional average PDSI and the NINO3.4 index in both monsoon regions (the time series of the moving correlation provided in Figure S3 in Supporting Information S1). We use these moving correlation coefficients to characterize changes in the ENSO–ASM relationship. As shown in the probability density function (PDF) of the moving correlations during 851–1950 C.E. (Figure 8), the ENSO–ASM relationship is non-stationary, but in most cases (over 70% of the correlations), average PDSI in both the EASM and ISM regions is negatively correlated with the NINO3.4 index. However, we note the proportion of significant negative correlations is less than 30% or even lower (see Table 1).

We determine the overall impact of the PDO/AMO on the ENSO–ASM teleconnection by comparing the PDF and means of the moving correlations during the whole period of 851–1950 C.E. with those during all the positive and negative phases of the PDO/AMO. Using 851–1950 C.E. as a reference period, the results of LMRv2.0 show that the mean ENSO–EASM and ENSO–ISM relationships are slightly weaker (stronger) during positive (negative) PDO phases (Figures 8a and 8b). Our findings are consistent with the recent studies that the weak ENSO–EASM correlations are associated with the El Niño-like sea surface temperature anomalies (Hu et al., 2023). However, the composite differences in correlations between positive and negative PDO phases are smaller than 0.05, and statistically insignificant. PHYDA indicates minimal changes (correlation changes smaller than 0.03, and statistically insignificant) in the mean moving correlations between positive and negative PDO phases for both the ENSO–EASM and ENSO–ISM relationship (Figures 8c and 8d). Similarly, the phase changes in AMO have an insignificant impact on the mean moving correlation coefficients of the ENSO–EASM and ENSO–ISM in both LMRv2.0 and PHYDA (Figure 9). It is worth noting that, regarding the ENSO–EASM relationship, LMRv2.0 exhibits an increased proportion of significant negative correlations during the negative (positive) phase of the PDO (AMO), whereas PHYDA shows the opposite (Figures 8 and 9, also Table 1). It is

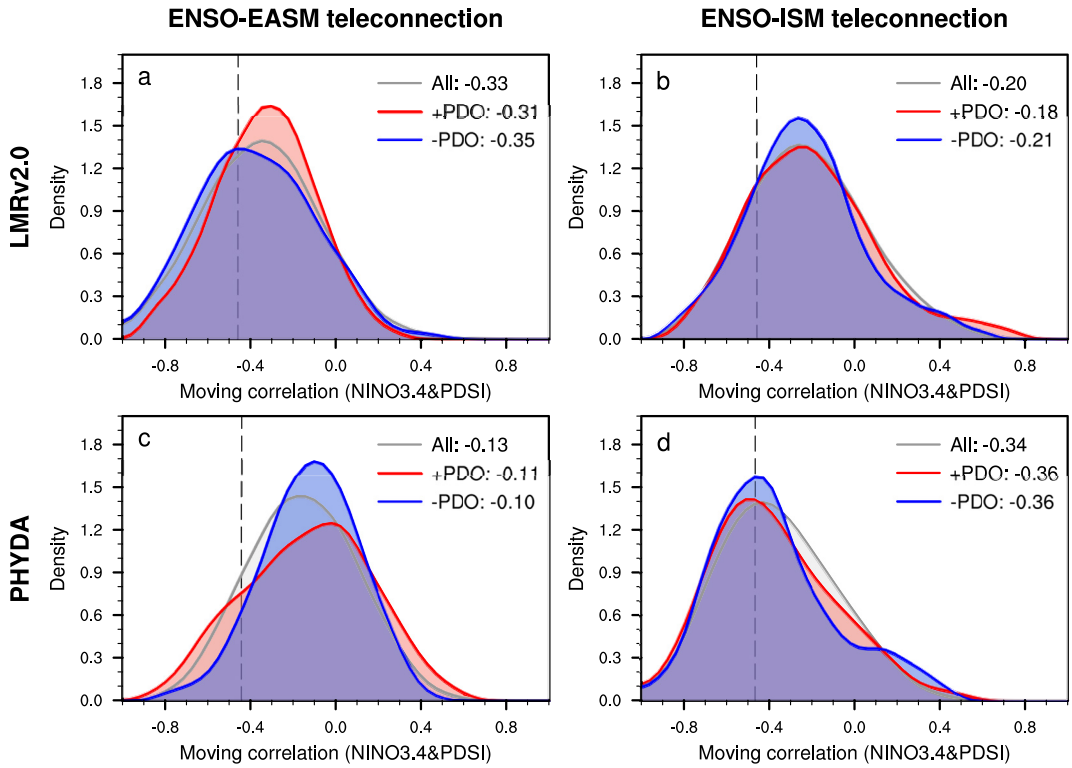

Figure 8. Changes in the ENSO–EASM and ENSO–ISM relationship between positive and negative PDO phases. Probability density function (PDF) of the 21-year moving correlation coefficients between the NINO3.4 index and regional mean PDSI over the (a, c) EASM regions, and (b, d) ISM regions during positive PDO (red), negative PDO (blue) phases, and all available years (gray, as the reference) for 851–1950 C.E., as calculated from (a, b) LMRv2.0, and (c, d) PHYDA. The mean values of the moving correlation coefficients are shown in the upper right corner. Changes in the mean moving correlations between positive and negative PDO phases lack statistical significance. Dash lines indicate the negative critical value for the 21-year correlation coefficient estimated by the averaged effective sample sizes over the past millennium given a 95% significance level.

thus not surprising that the two data sets show contrasting results regarding the PDO/AMO influence on the ENSO–monsoon covariability, since neither of them exhibits statistical significance.

The 21-year moving correlations between ENSO and the EASM in the CESM-LME are insignificant for the majority of the past millennium (Figures S15 and S17 in Supporting Information S1). Negative correlations between ENSO and the ISM are observed in most cases, with significant negative correlations detected in about one-third to half of the pool of correlation coefficients (Figures S16 and S18 in Supporting Information S1). However, the influence of PDO or AMO phase changes on the mean intensity of the ENSO–EASM and/or the ENSO–ISM teleconnection is insignificant in all ensemble members. Overall, LMRv2.0, PHYDA, and CESM-LME ensemble members consistently suggest the average influence of the PDO/AMO on the ENSO–ASM relationship over the last millennium is insignificant.

To interrogate this further, we conducted additional moving correlation analyses, connecting the 21-year moving correlation between the NINO3.4 and PDSI with the PDO and AMO indices on a longer sliding window of 101 years (Figure 10). For LMRv2.0, the period from 1000 C.E. to 1200 C.E. reveals noteworthy positive correlations between PDO and the 21-year moving correlation of ENSO–EASM (Figure 10a). Given the inverse ENSO–EASM relationships within this period (Figure S3 in Supporting Information S1), this suggests that when PDO transitions from negative to positive phases, the ENSO–EASM relationship weakens. However, during the period of 1250–1350 C.E., the correlation between PDO and the ENSO–EASM moving correlation turns negative, indicating that the transition of PDO from negative to positive phases strengthens the ENSO–EASM relationship. In the remaining periods throughout the past millennium in LMRv2.0, the association between PDO and ENSO–EASM covariability lacks statistical significance. Similarly, the relationship between PDO and the ENSO–ISM moving correlation also varies over time, with significant negative correlations occurring only

Table 1
Fraction of Negative ENSO–EASM and ENSO–ISM Correlations (Including Significant Negative Correlations in Italics) for 851–1950 C.E. and Those Under Different Backgrounds

ENSO–EASM	All	+PDO	−PDO	+AMO	−AMO
LMRv2.0	91%, 29%	94%, *22%*	94%, *35%*	92%, *43%*	87%, *23%*
PHYDA	72%, 8%	65%, *10%*	68%, *6%*	88%, *8%*	71%, *15%*
ENSO–ISM	**All**	**+PDO**	**−PDO**	**+AMO**	**−AMO**
LMRv2.0	79%, *14%*	79%, *12%*	84%, *14%*	68%, *11%*	69%, *14%*
PHYDA	89%, *30%*	89%, *34%*	86%, *36%*	83%, *16%*	88%, *18%*

Note. The ENSO–EASM and ENSO–ISM correlations refer to the 21-year moving correlations between the NINO3.4 index and regional mean PDSI over the EASM and ISM regions, respectively. In each unit, the first number indicates the fraction of negative correlations, while the second number represents the fraction of *significant negative correlations*. Red (blue) represents an increase (decrease) in the fraction of negative and *significant negative correlations* under different PDO or AMO backgrounds relative to the entire last millennium.

during the period of 1640–1740 C.E (Figure 10c). For PHYDA, a significant positive (negative) correlation between PDO and the ENSO–EASM moving correlation appears between 1170 and 1300 C.E. (1480–1600 C.E.); a significant negative correlation between PDO and the ENSO–ISM moving correlation is limited to between 1110 and 1210 C.E. (Figures 10b and 10d).

The relationship between AMO and the moving correlation of ENSO–ASM also exhibits temporal variations and disparities across data sets (Figures 10e–10h). In LMRv2.0, the relationship between AMO and the ENSO–EASM moving correlation is statistically insignificant throughout the past millennium. Significant negative (positive) correlations between AMO and the ENSO–ISM are observed during 1140–1240 C.E. (1470–1610 C.E.) in LMRv2.0. On the other hand, in PHYDA, a significant positive correlation between AMO and the ENSO–EASM moving correlation only appears during 1240–1340 C.E., and a significant positive correlation between AMO and ENSO–ISM is observed during 950–1050 C.E.; significant negative correlations are observed during 1100–1200 C.E. and 1300–1400 C.E.

The centennial-scale sliding window applied suggests that significant impacts of the PDO and AMO on the ENSO–ASM relationship have only manifested during a brief period within the past thousand years, and the occurrence does not exhibit clear regularity in terms of timing. This finding helps to explain the small difference in mean values of the ENSO–ASM moving correlations between all positive and negative phases of the PDO/AMO. The non-stationarity of the PDO/AMO modulating on the ENSO–ASM relationship is notable: while previous studies have indicated the potential influence of the PDO on the ENSO–monsoon covariability (Hau et al., 2023; Shi & Wang, 2019), few have been able to explore the non-stationarity over many centuries as we can with the Paleo-DA products.

3.5. Mechanisms of the PDO and AMO Impacts on the Asian Summer Monsoon

To elucidate the dynamics giving rise to PDO and AMO modulations of the ASM in the Paleo-DA, we perform composite analyses of SST, sea level pressure (SLP), and 500-hPa geopotential height fields provided in the Paleo-DA products. Note that PHYDA does not reconstruct geopotential height or other dynamical fields, and thus the circulation-related analysis is restricted to LMR 2.0. The results from Figures 11 and 12 support the interpretation that the PDO alters the impact of ENSO on the ASM because the spatial patterns of SST and circulation anomalies caused by these two modes of climate variability exhibit a high degree of consistency, despite differences in their time scales. For example, during El Niño events and positive PDO phases, warm SST anomalies occur in the central and eastern equatorial Pacific, whereas cold SST anomalies persist in the western Pacific and the Indian Ocean. Accordingly, the SLP in the central and eastern equatorial Pacific decreases, and SLP in the tropical western Pacific and over the Marine Continents increases. Previous studies indicate that this zonal SLP contrast causes the climatological mean Indo-Pacific Walker circulation to shift eastward, resulting in anomalous upward motions over the western Indian Ocean which stimulates anomalous descending motions and reduced precipitation in the ASM regions (Krishnamurthy & Goswami, 2000; Lau & Nath, 2003). Supporting this, the 500-hPa geopotential height field from LMRv2.0 (Figure 12) indicates that both positive PDO phases and El Niño events correspond to an anomalous anticyclonic circulation in the ASM region, consistent with a reduction of monsoon rainfall. Thus, when El Niño (La Niña) occurs with a positive (negative) PDO phase, the SST and circulation anomalies will be amplified, further strengthening the teleconnection and enhancing ASM precipitation anomalies. Conversely, when El Niño (La Niña) occurs with a negative (positive) PDO phase, the SST and circulation anomalies will be neutralized, reducing the magnitude of precipitation anomalies.

The SST patterns associated with the positive phase of the AMO are characterized by large-scale warming over the North Atlantic and eastern tropical Pacific (Figures 11c and 11f). From the reconstructed geopotential height field (Figure 12f), the warm SST anomalies in the North Atlantic trigger a circumglobal teleconnection (Ding & Wang, 2005; Wu, 2002), which propagates from the western North Atlantic to Asia. Anomalous cyclonic circulation occurs in the ASM regions, which favors increased precipitation. Consistent with the sea level pressure field (Figure 12c), warm SST anomalies in the eastern tropical Pacific result in an El Niño-like SLP gradient between the Indo-Pacific and eastern Pacific, leading to decreased precipitation in the ASM regions. It is evident that the warm anomalies

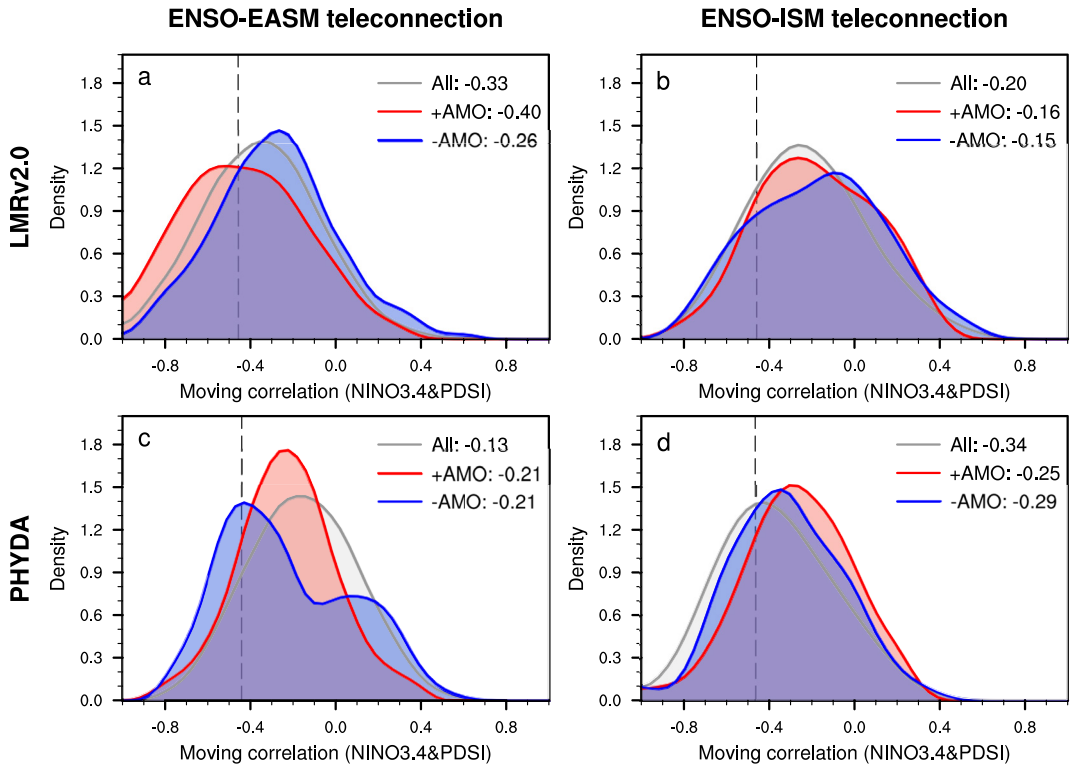

Figure 9. Same as in Figure 8, but for changes in the ENSO–EASM and ENSO–ISM relationship between positive and negative AMO phases. Changes in the mean moving correlations between positive and negative AMO phases lack statistical significance.

in the North Atlantic and the eastern tropical Pacific counterbalance each other in terms of precipitation anomalies, which helps to elucidate why the influence of the AMO phase change on the ASM is not significant in the paleo-data assimilations.

4. Discussion and Conclusions

This study used two paleoclimate data assimilation reconstructions, LMRv2.0 and PHYDA, to investigate how modes of (multi-)decadal climate variability modulate the ENSO–ASM relationship over the past millennium (851–1950 C.E.); specifically, we focused on (a) the compound effects of the PDO/AMO and ENSO on the ASM variability (Section 3.3) and (b) the influence of the PDO/AMO on the strength of the ENSO–ASM relationship (Section 3.4).

Both LMRv2.0 and PHYDA consistently show an overall inverse relationship between ENSO and the ASM during the past millennium (Figure 3). ENSO transitions from La Niña to El Niño events are associated with drier conditions over most of the ASM regions, including India, Southeast Asia, and northern China. The spatial pattern of the ASM response to the PDO resembles those of ENSO (Figure 4). When an El Niño occurs under a positive PDO phase, or a La Niña occurs under a negative PDO phase, the ASM anomalies caused by ENSO will be intensified, particularly in the ISM regions and Southeast Asia (Figure 5). Conversely, when an El Niño occurs under a negative PDO phase, or a La Niña occurs under a positive PDO phase, the ASM anomalies caused by ENSO will be weakened. In contrast, the phase changes of the AMO have little impact on the ASM (Figure 4), and the superposition of El Niño or La Niña events on the AMO does not result in significant changes in the ENSO–ASM teleconnection (Figure 6).

CESM-LME simulations exhibit general agreement with the Paleo-DA products regarding the ASM response to ENSO and PDO. For most of the CESM-LME ensemble members, the ASM precipitation anomalies associated with the compound effects of ENSO and the PDO or AMO are not significantly distinct from those induced by ENSO on average. Thus, while climate models show little distinction between the combined effects of the

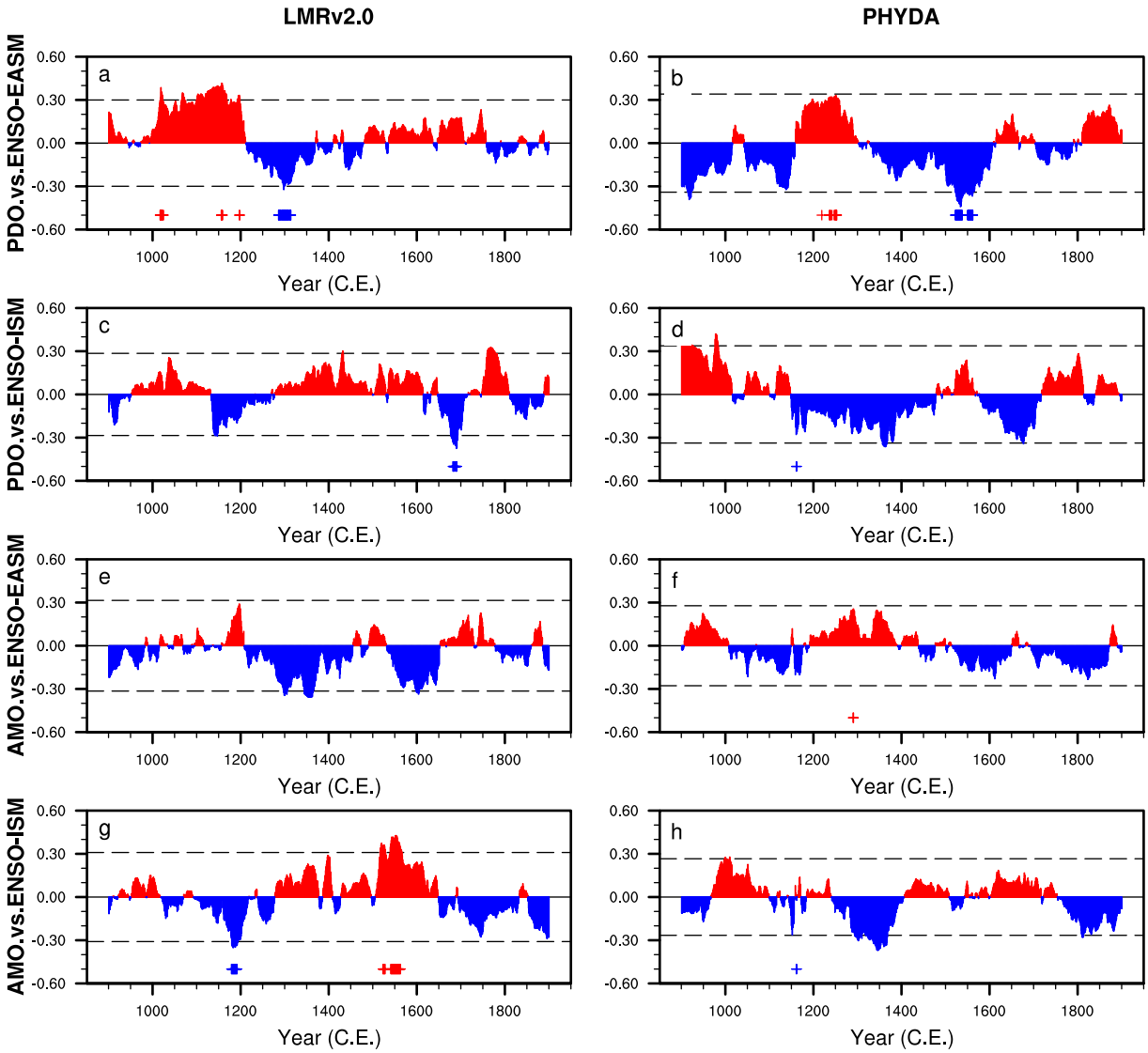

Figure 10. 101-year moving correlation between the PDO/AMO and the ENSO–ASM teleconnection. (a, b) Moving correlation between the PDO index and the ENSO–EASM teleconnection, (c, d) between the PDO index and the ENSO–ISM teleconnection, (e, f) between the AMO index and the ENSO–EASM teleconnection, (g, h) between the AMO index and the ENSO–ISM teleconnection for 851–1950 C.E. The left column is calculated from LMRv2.0, and the right column is from PHYDA. The ENSO–EASM and ENSO–ISM teleconnection is measured by the 21-year moving correlation between the NINO3.4 index and regional mean PDSI over the EASM and ISM regions. The dashed lines represent critical values for 101-year moving correlations. These values are estimated based on the averaged effective sample sizes over the past millennium, ensuring a 95% significance level according to the Student's *t*-test. The red (blue) crosses in the panel bottom indicate a significant positive (negative) correlation over a 101-year period centered on that year.

PDO/AMO and ENSO and the average effects of ENSO on the ASM, both Paleo-DA products incorporating proxy records confirm that when PDO occurs as the background of El Niño or La Niña, it can either enhance or weaken the impact of ENSO on the ISM.

Our analyses provide additional support for studies on the compound effects of PDO and ENSO on the ASM conducted using data spanning the instrumental period (Chan & Zhou, 2005; Krishnamurthy & Krishnamurthy, 2014). Notably, our study extends this work many hundreds of years into the past, providing a much larger sample of ENSO, PDO, and AMO events than the instrumental data alone. With the increased data pool afforded by the last millennium reconstructions, we can better disentangle the effects of the PDO and AMO by excluding the years when both PDO and AMO are strong and overlapping. We found that the individual influence of the PDO on ASM variability is much stronger than that of the AMO. This work thus underscores the power of utilizing Paleo-DA to shed light on the robust impact of (multi-)decadal-scale climate modes.

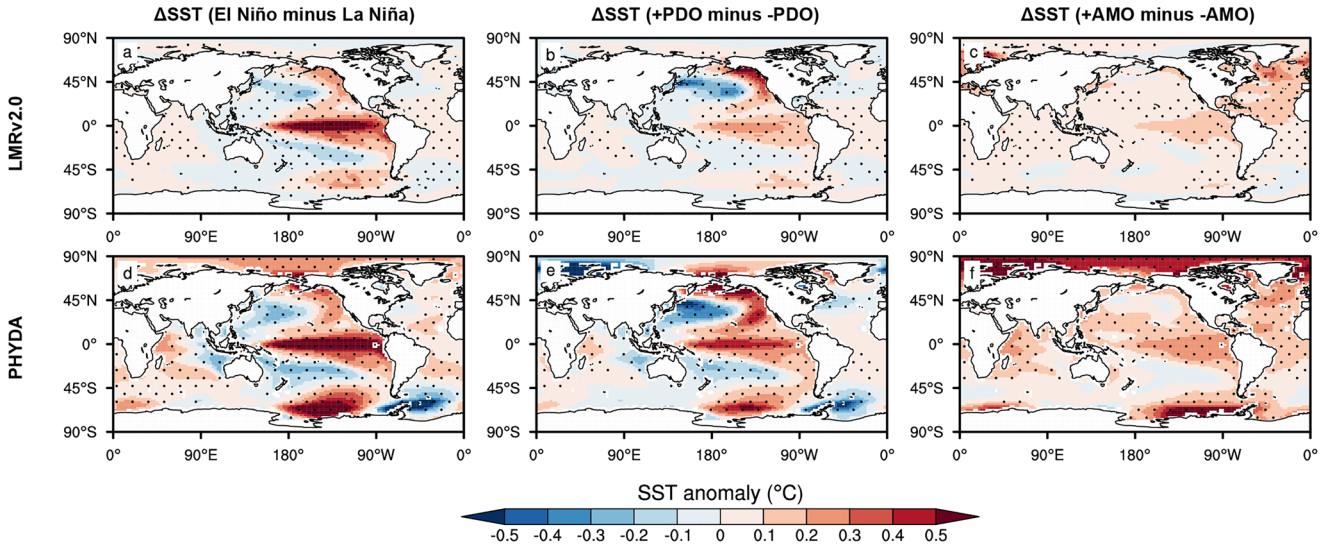

Figure 11. Sea surface temperature patterns related to ENSO, PDO, and AMO. Differences in sea surface temperature composites between (a, d) El Niño and La Niña events, (b, e) positive and negative PDO phases, and (c, f) positive and negative AMO phases for 851–1950 C.E., calculated from (a–c) LMRv2.0, and (d–f) PHYDA. Stippled areas denote significant differences at the 95% confidence level using the Student's *t*-test.

While the interdependence of PDO and ENSO phases is still an ongoing debate (Chen & Wallace, 2016; Newman et al., 2016; Vimont, 2005; Wills et al., 2018), we found that incorporating PDO in addition to ENSO cycles can remarkably enhance the prediction of the ISM in both data sets, but not the EASM in LMRv2.0 (Figure 7). The improvement in predicting the ISM is evident even when decadal-scale variability in ENSO cycles is not factored out. Our findings support a significant influence of extratropical variability on the ASM, as PDO results from multiple processes, encompassing both remote tropical forcing and local air-sea interactions in mid-latitudes (Newman et al., 2016).

The relationship between ENSO and the ASM (i.e., the strength of the teleconnection), as measured by the moving correlations between the NINO3.4 index and the regional mean PDSI over the ASM regions, was highly non-stationary over the last millennium. Through a comparison of the average ENSO–ASM relationships between all positive and negative phases of the PDO/AMO, we determined that the distinctions between positive and negative PDO/AMO phases are statistically insignificant (Figures 8 and 9). This lack of significance can

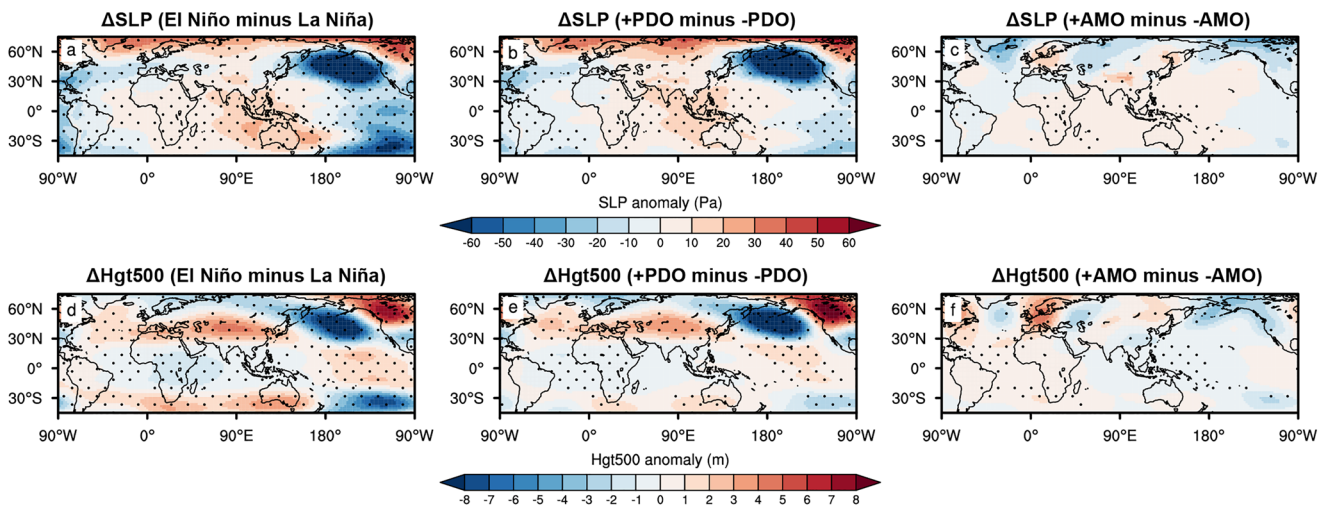

Figure 12. Sea level pressure and 500-hPa geopotential height patterns related to ENSO, PDO, and AMO. Differences in (a–c) sea level pressure and (d–f) 500-hPa geopotential height composites between (a, d) El Niño and La Niña events, (b, e) positive and negative PDO phases, and (c, f) positive and negative AMO phases for 851–1950 C.E., calculated from LMRv2.0 only. Stippled areas denote significant differences at the 95% confidence level using the Student's *t*-test.

be attributed to the fact that the impact of the PDO/AMO on the ENSO–ASM teleconnection also changes on centennial timescales, with notable influences only emerging during limited periods within the past millennium (Figure 10).

We acknowledge a few important caveats of this work. First, the method we use to define the AMO index is just one amongst various alternatives. Many previous studies subtract the global mean temperature when calculating the AMO index to remove the climate change signal for the instrumental era (Frajka-Williams et al., 2017; Si et al., 2021; Trenberth & Shea, 2006). We found that after defining the AMO index in this way, Paleo-DA products show negative SST anomalies in the tropical Pacific when the AMO is in a positive phase (Figures S19a and S19c in Supporting Information S1). This tends to trigger circulation patterns similar to La Niña events and results in increased rainfall in the EASM and ISM regions (Figures S19b and S19d in Supporting Information S1), which is consistent with conclusions based on observational data and model simulations (Krishnamurthy & Krishnamurthy, 2016; Li et al., 2008; Lu et al., 2006). Although different definitions of the AMO index can cause differences in the response of the ASM, the main conclusions of this study regarding the minimal impact of the AMO on the ENSO–ASM teleconnection remains robust.

While this study focuses on documenting the impact of (multi-)decadal-scale modes of climate variability on the ENSO–monsoon variation, it is crucial to acknowledge the significant impacts from external forcings. For instance, recent studies indicate that external forcings substantially influence the multidecadal-scale variability among the Atlantic sea surface temperatures, precipitation, and hurricane activity in surrounding regions (He et al., 2023). During the past millennium, solar radiation can modulate the impact of PDO on precipitation in eastern China (Xue et al., 2023). Furthermore, tropical volcanic eruptions can also affect the coupling between ENSO and the EASM on decadal scales (Zhu et al., 2022).

In addition, the Paleo-DA products only provide hydrological climate and SST reconstructions at an annual resolution. However, the ENSO–ASM relationships are seasonal and ENSO phase-dependent. For example, Wang et al. (2020) mentioned that the patterns of ENSO-induced rainfall anomalies in Asia vary across seasons. Additionally, the response of the EASM differs between the developing and decaying summers of El Niño. Thus, the dependence of the ASM response on different types of El Niño events, as well as the seasonal timing of those events, deserves further examination. Moreover, unfortunately, compared to North America and Europe, the available proxy records used for the data assimilation performed by both LMRv2.0 and PHYDA over Asia are very limited, which increases uncertainty in our study of variability of the East Asian monsoon using Paleo-DA to some extent. Future work must build paleoclimate data sets with higher temporal resolution and larger spatial coverage from this region; such work is sorely needed to help us better understand causes of changes in the ENSO–ASM relationship. Still, the additional information about past climate states at annual resolution afforded by the Paleo-DA products is critical for understanding the long-term behavior of the ASM in a warming climate.

This study takes a first step toward using paleoclimate reconstructions as a potential avenue for enhancing decadal-scale predictability of the ASM by analyzing the influence of both the AMO and PDO on the ENSO–ASM relationship. Past and future changes in the ASM have and will continue to impart severe consequences on agriculture, water resources, and natural disasters such as floods and droughts, affecting the livelihoods of billions of people. Studies such as this which can provide a larger sample size of coupled events linking modes of natural variability to better understand how climate modes will compound with anthropogenic forcing are critical for improving estimates of interannual variability in ASM rainfall. As decadal climate prediction continues to advance (Meehl et al., 2021; Smith et al., 2012, 2019), it is our hope that by clarifying the complex relationships between ENSO, the ASM, the PDO and AMO, this work may inform decision-making and mitigation of future ASM-related hazards and variability.

Conflict of Interest

The authors declare no conflicts of interest relevant to this study.

Data Availability Statement

All the data sets used in this analysis are publicly available.

LMRv2.0 (Tardif et al., 2019b): https://doi.org/10.25921/gn22-5866.

PHYDA (Steiger, 2018): https://doi.org/10.5281/zenodo.1198817.

CESM-LME (Kay et al., 2015): https://www.earthsystemgrid.org/dataset/ucar.cgd.ccsm4.cesmLME.html.

HadISST (Rayner et al., 2003): https://www.metoffice.gov.uk/hadobs/hadisst/data/download.html.

ERSSTv5 (Huang et al., 2017b): https://psl.noaa.gov/data/gridded/data.noaa.ersst.v5.html.

Global PDSI (Dai, 2017): https://doi.org/10.5065/D6QF8R93.

Acknowledgments
This work was supported by the National Science Foundation Paleoclimate Perspectives on Climate Change (P2C2) Award Number 2102814 to J.H. and S.D. and 2102812 to K.T. We appreciate Gregory Hakim and Nathan Steiger's assistance with accurate use and interpretation of LMR and PHYDA, and the CESM Paleoclimate Working Group at NCAR for the CESM-LME data availability.

References

Afyouni, S., Smith, S. M., & Nichols, T. E. (2019). Effective degrees of freedom of the Pearson's correlation coefficient under autocorrelation. *NeuroImage*, *199*, 609–625. https://doi.org/10.1016/j.neuroimage.2019.05.011

Anderson, D. M., Tardif, R., Horlick, K., Erb, M. P., Hakim, G. J., Noone, D., et al. (2019). Additions to the Last Millennium Reanalysis multi-proxy database. *Data Science Journal*, *18*(1), 2. https://doi.org/10.5334/dsj-2019-002

Aneesh, S., & Sijikumar, S. (2018). Changes in the La Niña teleconnection to the Indian summer monsoon during recent period. *Journal of Atmospheric and Solar-Terrestrial Physics*, *167*, 74–79. https://doi.org/10.1016/j.jastp.2017.11.009

Bhend, J., Franke, J., Folini, D., Wild, M., & Brönnimann, S. (2012). An ensemble-based approach to climate reconstructions. *Climate of the Past*, *8*(3), 963–976. https://doi.org/10.5194/cp-8-963-2012

Chakraborty, A., & Singhai, P. (2021). Asymmetric response of the Indian summer monsoon to positive and negative phases of major tropical climate patterns. *Scientific Reports*, *11*(1), 22561. https://doi.org/10.1038/s41598-021-01758-6

Chan, J. C. L., & Zhou, W. (2005). PDO, ENSO and the early summer monsoon rainfall over south China. *Geophysical Research Letters*, *32*(8). https://doi.org/10.1029/2004GL022015

Chen, W., Dong, B., & Lu, R. (2010). Impact of the Atlantic Ocean on the multidecadal fluctuation of El Niño–Southern Oscillation–South Asian monsoon relationship in a coupled general circulation model. *Journal of Geophysical Research*, *115*(D17), D17109. https://doi.org/10.1029/2009JD013596

Chen, X., & Wallace, J. M. (2016). Orthogonal PDO and ENSO indices. *Journal of Climate*, *29*(10), 3883–3892. https://doi.org/10.1175/JCLI-D-15-0684.1

Chen, Z., Zhou, T., Zhang, L., Chen, X., Zhang, W., & Jiang, J. (2020). Global land monsoon precipitation changes in CMIP6 projections. *Geophysical Research Letters*, *47*(14), e2019GL086902. https://doi.org/10.1029/2019GL086902

Chevuturi, A., Klingaman, N. P., Turner, A. G., & Hannah, S. (2018). Projected changes in the Asian-Australian monsoon region in 1.5°C and 2.0°C global-warming scenarios. *Earth's Future*, *6*(3), 339–358. https://doi.org/10.1002/2017EF000734

Cleveland, W. S. (1979). Robust locally weighted regression and smoothing scatterplots. *Journal of the American Statistical Association*, *74*(368), 829–836. https://doi.org/10.2307/2286407

Dai, A. (2011). Characteristics and trends in various forms of the Palmer Drought Severity Index during 1900–2008. *Journal of Geophysical Research*, *116*(D12), D12115. https://doi.org/10.1029/2010JD015541

Dai, A. (2017). Dai global palmer drought severity index (PDSI) [Dataset]. Research Data Archive at the National Center for Atmospheric Research, Computational and Information Systems Laboratory. https://doi.org/10.5065/D6QF8R93

Dee, S. G., Cobb, K. M., Emile-Geay, J., Ault, T. R., Edwards, R. L., Cheng, H., & Charles, C. D. (2020). No consistent ENSO response to volcanic forcing over the last millennium. *Science*, *367*(6485), 1477–1481. https://doi.org/10.1126/science.aax2000

Dee, S. G., & Steiger, N. J. (2022). ENSO's response to volcanism in a data assimilation-based paleoclimate reconstruction over the Common Era. *Paleoceanography and Paleoclimatology*, *37*(3). https://doi.org/10.1029/2021PA004290

Delworth, T. L., & Mann, M. E. (2000). Observed and simulated multidecadal variability in the Northern Hemisphere. *Climate Dynamics*, *16*(9), 661–676. https://doi.org/10.1007/s003820000075

Ding, Q., & Wang, B. (2005). Circumglobal teleconnection in the Northern Hemisphere summer. *Journal of Climate*, *18*(17), 3483–3505. https://doi.org/10.1175/JCLI3473.1

Ding, Y., & Chan, J. C. L. (2005). The East Asian summer monsoon: An overview. *Meteorology and Atmospheric Physics*, *89*(1–4), 117–142. https://doi.org/10.1007/s00703-005-0125-z

Dong, B., Sutton, R. T., & Scaife, A. A. (2006). Multidecadal modulation of El Niño–Southern Oscillation (ENSO) variance by Atlantic ocean sea surface temperatures. *Geophysical Research Letters*, *33*(8), L08705. https://doi.org/10.1029/2006GL025766

Du, X., Dee, S., Hu, J., & Thirumalai, K. (2023). Solar irradiance modulates the Asian summer monsoon—ENSO relationship over the last millennium. *Geophysical Research Letters*, *50*(23), e2023GL105708. https://doi.org/10.1029/2023gl105708

Emile-Geay, J., McKay, N. P., Kaufman, D. S., von Gunten, L., Wang, J., Anchukaitis, K. J., et al. (2017). A global multiproxy database for temperature reconstructions of the Common Era. *Scientific Data*, *4*(1), 170088. https://doi.org/10.1038/sdata.2017.88

Fan, F., Dong, X., Fang, X., Xue, F., Zheng, F., & Zhu, J. (2017). Revisiting the relationship between the South Asian summer monsoon drought and El Niño warming pattern. *Atmospheric Science Letters*, *18*(4), 175–182. https://doi.org/10.1002/asl.740

Fan, Y., Fan, K., Xu, Z., & Li, S. (2018). ENSO–South China Sea summer monsoon interaction modulated by the Atlantic Multidecadal Oscillation. *Journal of Climate*, *31*(8), 3061–3076. https://doi.org/10.1175/JCLI-D-17-0448.1

Frajka-Williams, E., Beaulieu, C., & Duchez, A. (2017). Emerging negative Atlantic Multidecadal Oscillation index in spite of warm subtropics. *Scientific Reports*, *7*(1), 11224. https://doi.org/10.1038/s41598-017-11046-x

Gadgil, S., & Rupa Kumar, K. (2006). The Asian monsoon—Agriculture and economy. In B. Wang (Ed.), *The Asian monsoon* (pp. 651–683). Springer. https://doi.org/10.1007/3-540-37722-0_18

George, G., Rao, D. N., Sabeerali, C. T., Srivastava, A., & Rao, S. A. (2016). Indian summer monsoon prediction and simulation in CFSv2 coupled model: Indian summer monsoon prediction and simulation in CFSv2 coupled model. *Atmospheric Science Letters*, *17*(1), 57–64. https://doi.org/10.1002/asl.599

Gershunov, A., Schneider, N., & Barnett, T. (2001). Low-frequency modulation of the ENSO–Indian monsoon rainfall relationship: Signal or noise? *Journal of Climate*, *14*(11), 2486–2492. https://doi.org/10.1175/1520-0442(2001)014<2486:LFMOTE>2.0.CO;2

Goosse, H., Guiot, J., Mann, M. E., Dubinkina, S., & Sallaz-Damaz, Y. (2012). The medieval climate anomaly in Europe: Comparison of the summer and annual mean signals in two reconstructions and in simulations with data assimilation. *Global and Planetary Change*, *84*(85), 35–47. https://doi.org/10.1016/j.gloplacha.2011.07.002

Goswami, B. N. (1998). Interannual variations of Indian summer monsoon in a GCM: External conditions versus internal feedbacks. *Journal of Climate*, *11*(4), 501–522. https://doi.org/10.1175/1520-0442(1998)011<0501:IVOISM>2.0.CO;2

Goswami, B. N., Wu, G., & Yasunari, T. (2006). The annual cycle, intraseasonal oscillations, and roadblock to seasonal predictability of the Asian summer monsoon. *Journal of Climate*, *19*(20), 5078–5099. https://doi.org/10.1175/JCLI3901.1

Ha, K.-J., Seo, Y.-W., Lee, J.-Y., Kripalani, R. H., & Yun, K.-S. (2018). Linkages between the South and East Asian summer monsoons: A review and revisit. *Climate Dynamics*, *51*(11), 4207–4227. https://doi.org/10.1007/s00382-017-3773-z

Hakim, G. J., Emile-Geay, J., Steig, E. J., Noone, D., Anderson, D. M., Tardif, R., et al. (2016). The last millennium climate reanalysis project: Framework and first results. *Journal of Geophysical Research: Atmospheres*, *121*(12), 6745–6764. https://doi.org/10.1002/2016JD024751

Hau, N.-X., Sano, M., Nakatsuka, T., Chen, S.-H., & Chen, I.-C. (2023). The modulation of Pacific Decadal Oscillation on ENSO-East Asian summer monsoon relationship over the past half-millennium. *Science of the Total Environment*, *857*, 159437. https://doi.org/10.1016/j.scitotenv.2022.159437

He, C., Clement, A. C., Kramer, S. M., Cane, M. A., Klavans, J. M., Fenske, T. M., & Murphy, L. N. (2023). Tropical Atlantic multidecadal variability is dominated by external forcing. *Nature*, *622*(7983), 521–527. https://doi.org/10.1038/s41586-023-06489-4

Hrudya, P. H., Varikoden, H., & Vishnu, R. (2021). A review on the Indian summer monsoon rainfall, variability and its association with ENSO and IOD. *Meteorology and Atmospheric Physics*, *133*(1), 1–14. https://doi.org/10.1007/s00703-020-00734-5

Hsu, H.-H., Zhou, T., & Matsumoto, J. (2014). East Asian, Indochina and western North Pacific Summer monsoon—An update. *Asia-Pacific Journal of Atmospheric Sciences*, *50*(1), 45–68. https://doi.org/10.1007/s13143-014-0027-4

Hsu, P., Li, T., Murakami, H., & Kitoh, A. (2013). Future change of the global monsoon revealed from 19 CMIP5 models. *Journal of Geophysical Research: Atmospheres*, *118*(3), 1247–1260. https://doi.org/10.1002/jgrd.50145

Hu, J., Dee, S., Parajuli, G., & Thirumalai, K. (2023). Tropical Pacific modulation of the Asian summer monsoon over the last millennium in paleoclimate data assimilation reconstructions. *Journal of Geophysical Research: Atmospheres*, *128*(20), e2023JD039207. https://doi.org/10.1029/2023JD039207

Hu, P., Chen, W., Wang, L., Chen, S., Liu, Y., & Chen, L. (2022). Revisiting the ENSO–monsoonal rainfall relationship: New insights based on an objective determination of the Asian summer monsoon duration. *Environmental Research Letters*, *17*(10), 104050. https://doi.org/10.1088/1748-9326/ac97ad

Huang, B., Thorne, P. W., Banzon, V. F., Boyer, T., Chepurin, G., Lawrimore, J. H., et al. (2017a). Extended reconstructed sea surface temperature, version 5 (ERSSTv5): Upgrades, validations, and intercomparisons. *Journal of Climate*, *30*(20), 8179–8205. https://doi.org/10.1175/JCLI-D-16-0836.1

Huang, B., Thorne, P. W., Banzon, V. F., Boyer, T., Chepurin, G., Lawrimore, J. H., et al. (2017b). NOAA extended reconstructed sea surface temperature (ERSST), version 5 [Dataset]. NOAA National Centers for Environmental Information. Obtain at NOAA/ESRL/PSD at their website. https://doi.org/10.7289/V5T72FNM

Jin, C., Liu, J., Wang, B., Yan, M., & Ning, L. (2019). Decadal variations of the East Asian summer monsoon forced by the 11-year insolation cycle. *Journal of Climate*, *32*(10), 2735–2745. https://doi.org/10.1175/JCLI-D-18-0288.1

Katzenberger, A., Schewe, J., Pongratz, J., & Levermann, A. (2021). Robust increase of Indian monsoon rainfall and its variability under future warming in CMIP6 models. *Earth System Dynamics*, *12*(2), 367–386. https://doi.org/10.5194/esd-12-367-2021

Kay, J. E., Deser, C., Phillips, A., Mai, A., Hannay, C., Strand, G., et al. (2015). The Community Earth System Model (CESM) large ensemble project: A community resource for studying climate change in the presence of internal climate variability [Dataset]. Bulletin of the American Meteorological Society, *96*, 1333–1349. https://doi.org/10.1175/BAMS-D-13-00255.1

Kim, M.-K., Lau, W. K. M., Kim, K.-M., Sang, J., Kim, Y.-H., & Lee, W.-S. (2016). Amplification of ENSO effects on Indian summer monsoon by absorbing aerosols. *Climate Dynamics*, *46*(7), 2657–2671. https://doi.org/10.1007/s00382-015-2722-y

Kripalani, R. h., & Kulkarni, A. (2001). Monsoon rainfall variations and teleconnections over South and East Asia. *International Journal of Climatology*, *21*(5), 603–616. https://doi.org/10.1002/joc.625

Krishnamurthy, L., & Krishnamurthy, V. (2014). Influence of PDO on South Asian summer monsoon and monsoon–ENSO relation. *Climate Dynamics*, *42*(9–10), 2397–2410. https://doi.org/10.1007/s00382-013-1856-z

Krishnamurthy, L., & Krishnamurthy, V. (2016). Teleconnections of Indian monsoon rainfall with AMO and Atlantic tripole. *Climate Dynamics*, *46*(7), 2269–2285. https://doi.org/10.1007/s00382-015-2701-3

Krishnamurthy, V., & Goswami, B. N. (2000). Indian Monsoon–ENSO relationship on interdecadal timescale. *Journal of Climate*, *13*(3), 579–595. https://doi.org/10.1175/1520-0442(2000)013<0579:IMEROI>2.0.CO;2

Krishnan, R., & Sugi, M. (2003). Pacific decadal oscillation and variability of the Indian summer monsoon rainfall. *Climate Dynamics*, *21*(3–4), 233–242. https://doi.org/10.1007/s00382-003-0330-8

Kumar, K. K., Rajagopalan, B., & Cane, M. A. (1999). On the weakening relationship between the Indian monsoon and ENSO. *Science*, *284*(5423), 2156–2159. https://doi.org/10.1126/science.284.5423.2156

Kumar, K. K., Rajagopalan, B., Hoerling, M., Bates, G., & Cane, M. (2006). Unraveling the mystery of Indian monsoon failure during El Niño. *Science*, *314*(5796), 115–119. https://doi.org/10.1126/science.1131152

Landrum, L., Otto-Bliesner, B. L., Wahl, E. R., Conley, A., Lawrence, P. J., Rosenbloom, N., & Teng, H. (2013). Last millennium climate and its variability in CCSM4. *Journal of Climate*, *26*(4), 1085–1111. https://doi.org/10.1175/JCLI-D-11-00326.1

Lau, N.-C., & Nath, M. J. (2000). Impact of ENSO on the variability of the Asian–Australian monsoons as simulated in GCM experiments. *Journal of Climate*, *13*(24), 4287–4309. https://doi.org/10.1175/1520-0442(2000)013<4287:IOEOTV>2.0.CO;2

Lau, N.-C., & Nath, M. J. (2003). Atmosphere–Ocean variations in the Indo-Pacific Sector during ENSO episodes. *Journal of Climate*, *16*(1), 3–20. https://doi.org/10.1175/1520-0442(2003)016<0003:aoviti>2.0.co;2

Li, S., Perlwitz, J., Quan, X., & Hoerling, M. P. (2008). Modelling the influence of North Atlantic multidecadal warmth on the Indian summer rainfall. *Geophysical Research Letters*, *35*(5), L05804. https://doi.org/10.1029/2007GL032901

Liu, X., Yang, S., Kumar, A., Weaver, S., & Jiang, X. (2013). Diagnostics of subseasonal prediction biases of the Asian summer monsoon by the NCEP climate forecast system. *Climate Dynamics*, *41*(5), 1453–1474. https://doi.org/10.1007/s00382-012-1553-3

Lu, R., Dong, B., & Ding, H. (2006). Impact of the Atlantic Multidecadal Oscillation on the Asian summer monsoon. *Geophysical Research Letters*, *33*(24). https://doi.org/10.1029/2006GL027655

Luo, X., Dee, S., Lavenhouse, T., Muñoz, S., & Steiger, N. (2023). Tropical Pacific and North Atlantic sea surface temperature patterns modulate Mississippi basin hydroclimate extremes over the last millennium. *Geophysical Research Letters*, *50*(2), e2022GL100715. https://doi.org/10.1029/2022GL100715

Luo, X., Dee, S., Stevenson, S., Okumura, Y., Steiger, N., & Parsons, L. (2022). Last millennium ENSO diversity and North American teleconnections: New insights from paleoclimate data assimilation. *Paleoceanography and Paleoclimatology*, *37*(3). https://doi.org/10.1029/2021PA004283

Madolli, M. J., Himanshu, S. K., Patro, E. R., & De Michele, C. (2022). Past, present and future perspectives of seasonal prediction of Indian summer monsoon rainfall: A review. *Asia-Pacific Journal of Atmospheric Sciences*, *58*(4), 591–615. https://doi.org/10.1007/s13143-022-00273-6

Mantua, N. J., Hare, S. R., Zhang, Y., Wallace, J. M., & Francis, R. C. (1997). A Pacific interdecadal climate oscillation with impacts on salmon production. *Bulletin of the American Meteorological Society*, *78*(6), 1069–1080. https://doi.org/10.1175/1520-0477(1997)078<1069:APICOW>2.0.CO;2

McGregor, S., Cassou, C., Kosaka, Y., & Phillips, A. S. (2022). Projected ENSO teleconnection changes in CMIP6. *Geophysical Research Letters*, *49*(11), e2021GL097511. https://doi.org/10.1029/2021GL097511

Meehl, G. A., Richter, J. H., Teng, H., Capotondi, A., Cobb, K., Doblas-Reyes, F., et al. (2021). Initialized Earth system prediction from subseasonal to decadal timescales. *Nature Reviews Earth & Environment*, *2*(5), 340–357. https://doi.org/10.1038/s43017-021-00155-x

Mehta, V. M., & Lau, K.-M. (1997). Influence of solar irradiance on the Indian Monsoon-ENSO relationship at decadal-multidecadal time scales. *Geophysical Research Letters*, *24*(2), 159–162. https://doi.org/10.1029/96GL03778

Mishra, V., Smoliak, B. V., Lettenmaier, D. P., & Wallace, J. M. (2012). A prominent pattern of year-to-year variability in Indian Summer Monsoon Rainfall. *Proceedings of the National Academy of Sciences of the United States of America*, *109*(19), 7213–7217. https://doi.org/10.1073/pnas.1119150109

Narasimha, R., & Bhattacharyya, S. (2010). A wavelet cross-spectral analysis of solar–ENSO–rainfall connections in the Indian monsoons. *Applied and Computational Harmonic Analysis*, *28*(3), 285–295. https://doi.org/10.1016/j.acha.2010.02.005

Newman, M., Alexander, M. A., Ault, T. R., Cobb, K. M., Deser, C., Lorenzo, E. D., et al. (2016). The Pacific decadal oscillation, revisited. *Journal of Climate*, *29*(12), 4399–4427. https://doi.org/10.1175/JCLI-D-15-0508.1

Otto-Bliesner, B. L., Brady, E. C., Fasullo, J., Jahn, A., Landrum, L., Stevenson, S., et al. (2016). Climate variability and change since 850 CE: An ensemble approach with the community earth system model. *Bulletin of the American Meteorological Society*, *97*(5), 735–754. https://doi.org/10.1175/BAMS-D-14-00233.1

Palmer, W. C. (1965). *Meteorological drought. Res. Paper No.45* (p. 58). Department of Commerce.

Pandey, P., Dwivedi, S., Goswami, B. N., & Kucharski, F. (2020). A new perspective on ENSO-Indian summer monsoon rainfall relationship in a warming environment. *Climate Dynamics*, *55*(11), 3307–3326. https://doi.org/10.1007/s00382-020-05452-7

Rani, S. I., Arulalan, T., George, J. P., Rajagopal, E. N., Renshaw, R., Maycock, A., et al. (2021). IMDAA: High-resolution satellite-era reanalysis for the Indian monsoon region. *Journal of Climate*, *34*(12), 5109–5133. https://doi.org/10.1175/JCLI-D-20-0412.1

Rayner, N. A., Parker, D. E., Horton, E. B., Folland, C. K., Alexander, L. V., Rowell, D. P., et al. (2003). Global analyses of sea surface temperature, sea ice, and night marine air temperature since the late nineteenth century [Dataset]. Journal of Geophysical Research, *108*. https://doi.org/10.1029/2002JD002670

Roy, I., Tedeschi, R. G., & Collins, M. (2019). ENSO teleconnections to the Indian summer monsoon under changing climate. *International Journal of Climatology*, *39*(6), 3031–3042. https://doi.org/10.1002/joc.5999

Shi, H., & Wang, B. (2019). How does the Asian summer precipitation-ENSO relationship change over the past 544 years? *Climate Dynamics*, *52*(7), 4583–4598. https://doi.org/10.1007/s00382-018-4392-z

Si, D., Jiang, D., Hu, A., & Lang, X. (2021). Variations in northeast Asian summer precipitation driven by the Atlantic multidecadal oscillation. *International Journal of Climatology*, *41*(3), 1682–1695. https://doi.org/10.1002/joc.6912

Singh, M., Krishnan, R., Goswami, B., Choudhury, A. D., Swapna, P., Vellore, R., et al. (2020). Fingerprint of volcanic forcing on the ENSO–Indian monsoon coupling. *Science Advances*, *6*(38), eaba8164. https://doi.org/10.1126/sciadv.aba8164

Smith, D. M., Eade, R., Scaife, A. A., Caron, L.-P., Danabasoglu, G., DelSole, T. M., et al. (2019). Robust skill of decadal climate predictions. *Npj Climate and Atmospheric Science*, *2*(1), 1–10. https://doi.org/10.1038/s41612-019-0071-y

Smith, D. M., Scaife, A. A., & Kirtman, B. P. (2012). What is the current state of scientific knowledge with regard to seasonal and decadal forecasting? *Environmental Research Letters*, *7*(1), 015602. https://doi.org/10.1088/1748-9326/7/1/015602

Steiger, N. J. (2018). Paleo hydrodynamics data assimilation product (PHYDA) [Dataset]. Zenodo. https://doi.org/10.5281/zenodo.1198817

Steiger, N. J., Hakim, G. J., Steig, E. J., Battisti, D. S., & Roe, G. H. (2014). Assimilation of time-averaged pseudoproxies for climate reconstruction. *Journal of Climate*, *27*(1), 426–441. https://doi.org/10.1175/JCLI-D-12-00693.1

Steiger, N. J., Smerdon, J. E., Cook, E. R., & Cook, B. I. (2018). A reconstruction of global hydroclimate and dynamical variables over the Common Era. *Scientific Data*, *5*(1), 180086. https://doi.org/10.1038/sdata.2018.86

Steiger, N. J., Smerdon, J. E., Seager, R., Williams, A. P., & Varuolo-Clarke, A. M. (2021). ENSO-driven coupled megadroughts in North and South America over the last millennium. *Nature Geoscience*, *14*(10), 739–744. https://doi.org/10.1038/s41561-021-00819-9

Tang, Y., Zhang, R.-H., Liu, T., Duan, W., Yang, D., Zheng, F., et al. (2018). Progress in ENSO prediction and predictability study. *National Science Review*, *5*(6), 826–839. https://doi.org/10.1093/nsr/nwy105

Tardif, R., Hakim, G. J., Perkins, W. A., Horlick, K. A., Erb, M. P., Emile-Geay, J., et al. (2019a). Last Millennium Reanalysis with an expanded proxy database and seasonal proxy modeling. *Climate of the Past*, *15*(4), 1251–1273. https://doi.org/10.5194/cp-15-1251-2019

Tardif, R., Hakim, G. J., Perkins, W. A., Horlick, K. A., Erb, M. P., Emile-Geay, J., et al. (2019b). NOAA/WDS paleoclimatology—Last millennium reanalysis (LMR) project global climate reconstructions version 2 [Dataset]. NOAA National Centers for Environmental Information. https://doi.org/10.25921/gn22-5866

Tejedor, E., Steiger, N., Smerdon, J. E., Serrano-Notivoli, R., & Vuille, M. (2021). Global temperature responses to large tropical volcanic eruptions in paleo data assimilation products and climate model simulations over the last millennium. *Paleoceanography and Paleoclimatology*, *36*(4), e2020PA004128. https://doi.org/10.1029/2020PA004128

Trenberth, K. E. (1997). The definition of El Niño. *Bulletin of the American Meteorological Society*, *78*(12), 2771–2778. https://doi.org/10.1175/1520-0477(1997)078<2771:TDOENO>2.0.CO;2

Trenberth, K. E., Hurrell, J. W., & Stepaniak, D. P. (2006). The Asian monsoon: Global perspectives. In B. Wang (Ed.), *The Asian monsoon* (pp. 67–87). Springer. https://doi.org/10.1007/3-540-37722-0_2

Trenberth, K. E., & Shea, D. J. (2006). Atlantic hurricanes and natural variability in 2005. *Geophysical Research Letters*, *33*(12). https://doi.org/10.1029/2006GL026894

Vimont, D. J. (2005). The contribution of the interannual ENSO cycle to the spatial pattern of decadal ENSO-like variability. *Journal of Climate*, *18*(12), 2080–2092. https://doi.org/10.1175/JCLI3365.1

Wang, B., & LinHo (2002). Rainy season of the Asian–Pacific summer monsoon. *Journal of Climate*, *15*(4), 386–398. https://doi.org/10.1175/1520-0442(2002)015<0386:RSOTAP>2.0.CO;2

Wang, B., Luo, X., & Liu, J. (2020). How robust is the Asian precipitation–ENSO relationship during the industrial warming period (1901–2017)? *Journal of Climate*, *33*(7), 2779–2792. https://doi.org/10.1175/JCLI-D-19-0630.1

Wang, B., Wu, R., & Lau, K.-M. (2001). Interannual variability of the Asian summer monsoon: Contrasts between the Indian and the western North Pacific–East Asian monsoons. *Journal of Climate*, *14*(20), 4073–4090. https://doi.org/10.1175/1520-0442(2001)014<4073:IVOTAS>2.0.CO;2

Wang, B., Wu, Z., Li, J., Liu, J., Chang, C.-P., Ding, Y., & Wu, G. (2008). How to measure the strength of the East Asian summer monsoon. *Journal of Climate*, *21*(17), 4449–4463. https://doi.org/10.1175/2008JCLI2183.1

Wang, B., Yim, S.-Y., Lee, J.-Y., Liu, J., & Ha, K.-J. (2014). Future change of Asian-Australian monsoon under RCP 4.5 anthropogenic warming scenario. *Climate Dynamics*, *42*(1), 83–100. https://doi.org/10.1007/s00382-013-1769-x

Wang, T., Miao, J.-P., Sun, J.-Q., & Fu, Y.-H. (2018). Intensified East Asian summer monsoon and associated precipitation mode shift under the 1.5°C global warming target. *Advances in Climate Change Research*, *9*(2), 102–111. https://doi.org/10.1016/j.accre.2017.12.002

Webster, P. J., Magaña, V. O., Palmer, T. N., Shukla, J., Tomas, R. A., Yanai, M., & Yasunari, T. (1998). Monsoons: Processes, predictability, and the prospects for prediction. *Journal of Geophysical Research*, *103*(C7), 14451–14510. https://doi.org/10.1029/97JC02719

Webster, P. J., & Yang, S. (1992). Monsoon and ENSO: Selectively interactive systems. *Quarterly Journal of the Royal Meteorological Society*, *118*(507), 877–926. https://doi.org/10.1002/qj.49711850705

Widmann, M., Goosse, H., van der Schrier, G., Schnur, R., & Barkmeijer, J. (2010). Using data assimilation to study extratropical Northern Hemisphere climate over the last millennium. *Climate of the Past*, *6*(5), 627–644. https://doi.org/10.5194/cp-6-627-2010

Wills, R. C., Schneider, T., Wallace, J. M., Battisti, D. S., & Hartmann, D. L. (2018). Disentangling global warming, multidecadal variability, and El Niño in Pacific temperatures. *Geophysical Research Letters*, *45*(5), 2487–2496. https://doi.org/10.1002/2017GL076327

Wu, R. (2002). A mid-latitude Asian circulation anomaly pattern in boreal summer and its connection with the Indian and East Asian summer monsoons. *International Journal of Climatology*, *22*(15), 1879–1895. https://doi.org/10.1002/joc.845

Xu, C., Wang, S.-Y. S., Borhara, K., Buckley, B., Tan, N., Zhao, Y., et al. (2023). Asian-Australian summer monsoons linkage to ENSO strengthened by global warming. *Npj Climate and Atmospheric Science*, *6*(1), 1–9. https://doi.org/10.1038/s41612-023-00341-2

Xu, M., Xu, H., Ma, J., & Deng, J. (2023). Modulation of Atlantic Multidecadal Oscillation on ENSO-East Asian early summer monsoon connection: Role of a tropical pathway. *Climate Dynamics*, *61*(9–10), 4301–4318. https://doi.org/10.1007/s00382-023-06811-w

Xue, J., Ning, L., Liu, Z., Qin, Y., Chen, K., Yan, M., et al. (2023). The combined influences of solar radiation and PDO on precipitation over eastern China during the last millennium. *Climate Dynamics*, *60*(3), 1137–1150. https://doi.org/10.1007/s00382-022-06372-4

Yang, Q., Ma, Z., Fan, X., Yang, Z.-L., Xu, Z., & Wu, P. (2017). Decadal modulation of precipitation patterns over eastern China by sea surface temperature anomalies. *Journal of Climate*, *30*(17), 7017–7033. https://doi.org/10.1175/JCLI-D-16-0793.1

Yang, X., & Huang, P. (2021). Restored relationship between ENSO and Indian summer monsoon rainfall around 1999/2000. *Innovation*, *2*(2), 100102. https://doi.org/10.1016/j.xinn.2021.100102

Yu, S.-Y., Fan, L., Zhang, Y., Zheng, X.-T., & Li, Z. (2021). Reexamining the Indian summer monsoon rainfall–ENSO relationship from its recovery in the 21st century: Role of the Indian Ocean sst anomaly associated with types of ENSO evolution. *Geophysical Research Letters*, *48*(12), e2021GL092873. https://doi.org/10.1029/2021GL092873

Yun, K.-S., & Timmermann, A. (2018). Decadal Monsoon-ENSO relationships reexamined. *Geophysical Research Letters*, *45*(4), 2014–2021. https://doi.org/10.1002/2017GL076912

Zhang, Y., Wallace, J. M., & Battisti, D. S. (1997). ENSO-Like interdecadal variability: 1900–93. *Journal of Climate*, *10*(5), 1004–1020. https://doi.org/10.1175/1520-0442(1997)010<1004:ELIV>2.0.CO;2

Zhu, J., Zhao, K., Wang, Y., Cui, Y., Liang, Y., Cheng, H., et al. (2022). Decadal modulation of East Asian summer monsoon variations by external forcing and internal variability. *Quaternary Science Reviews*, *293*, 107720. https://doi.org/10.1016/j.quascirev.2022.107720

Zwiers, F. W., & Von Storch, H. (1995). Taking serial correlation into account in tests of the mean. *Journal of Climate*, *8*(2), 336–351. https://doi.org/10.1175/1520-0442(1995)008<0336:TSCIAI>2.0.CO;2